Deliverable D 4.4
Thermomechanical characterisation of 3D pilot model finished

Document type	**Deliverable D 4.4**
Document Version / Status	**1.6**
Primary Authors	**João Pereira,** jpereira@civil.uminho.pt, **UMINHO**
Distribution Level	**PU (Public)**
Project Acronym	**ATHOR**
Project Title	**Advanced THermomechanical multiscale mOdelling of Refractory linings**
Grant Agreement Number	**764987**
Project Website	www.etn-athor.eu
Project Coordinator	**Marc Huger,** marc.huger@unilim.fr, **UNILIM**
Document Contributors	**João Pereira,** jpereira@civil.uminho.pt, **UMINHO** **Pratik Gajjar,** pratik.gajjar@civil.uminho.pt, **UMINHO** **Pieter Put,** pieter.put@tatasteeleurope.com, **TATA** **Sido Sinnema,** sido.sinnema@tatasteeleurope.com, **TATA**

History of Changes

Version	Date	Author (Organization)	Change	Page
1.0	06.03.2022	Pratik GAJJAR (UMINHO)	First version of the deliverable created	All
1.1	09.03.2022	João Pereira (UMINHO)	Review	All
1.2	09.03.2022	Pratik GAJJAR (UMINHO)	Revision	All
1.3	10.03.2022	Pratik GAJJAR (UMINHO)	Revision	All
1.4	17.03.2022	João Pereira (UMINHO)	Review	All
1.5	21.03.2022	Glyn Derrick (UNILIM)	English and formatting check	All
1.6	29.03.2022	Glyn Derrick (UNILIM) Marc HUGER (UNILIM)	Final Check	All

European Commission
Horizon 2020
European Union funding
for Research & Innovation

TABLE OF CONTENTS

1 Introduction

Refractory materials exhibit complex behaviour. At lower temperatures, their behaviour is brittle, while at high temperatures, it becomes ductile [1]. The importance of creep for refractories in industrial applications has been shown in previous research [2][3]. The same can be described for the corrosion of refractories [4][5]. These materials are used in large installations, which adds more complexity, such as joint behaviour [6][7]. Therefore, developing a coherent modelling approach requires experiments at large-scale. Such tests are rarely performed due to the high cost involved, and when successful, they have been mainly done on masonry walls [8][9][10].

With the objective of gathering data for the validation of advanced numerical models, experimental characterisation of the refractory masonry that undergoes similar thermomechanical loadings as an industrial ladle was deemed necessary. Within ATHOR, an unprecedented experimental installation was envisaged – a 3D pilot ladle. This represents a novel approach towards designing an experimental setup for large-scale refractory masonry. It requires original test configuration, from designing the geometry, insulation, heating requirement, measurement devices, and installation.

This 3D pilot model is a scaled representation of a ladle (Figure 1), which includes all the linings as an industrial ladle and is expected to be tested under the thermal loads of similar magnitude of an industrial ladle without the presence of molten steel which will also allow to characterise and monitor the inner surface of the linings mechanically. The construction and testing of this experimental device will be at the Ceramics Research Centre (CRC) of Tata Steel in Ijmuiden, Netherland.

This document gathers all the information regarding the development of such application. First the design of the pilot is described, including all the consideration taken throughout all stages of design. This stage required the development of several numerical campaigns. The second phase was the design of the insulation and heating elements. Here, several considerations regarding the bottom, lid and distribution of the heating elements were made. The third phase is the identification and design of the acquisition systems to be installed within the pilot. Here, both thermal as well as mechanical measurements were considered. The final phase is the presentation of the current state of the installation.

European Commission | Horizon 2020 European Union funding for Research & Innovation

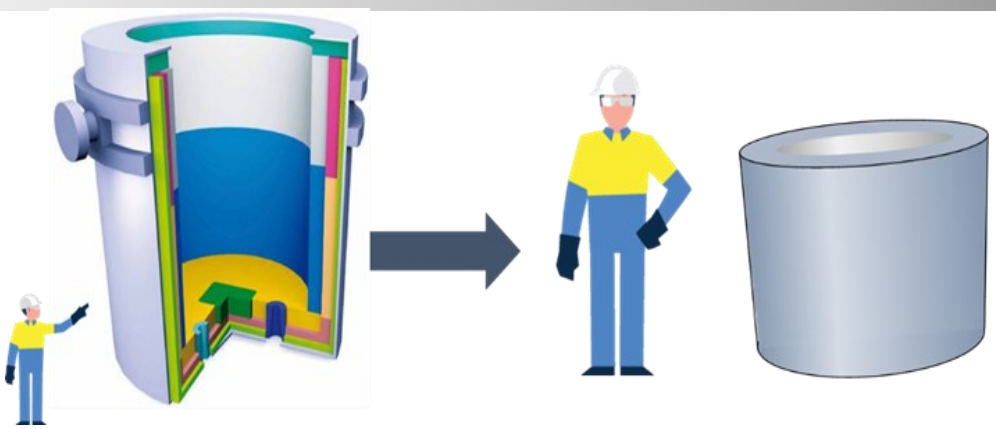

Figure 1 - Graphical representation of the laboratory scaled steel ladle

It should be noted that the objective was to present within this document all the experimental results obtained with such experimental campaign. However, due to the COVID pandemic, the work within this task was delayed to a point where the experimental results are not available within the timeframe of ATHOR (March 2022). It should be also noted that extra funding was procured to fund the ESR responsible for the development of this work (at UMinho, for 18 extra months). The Partner Organization involved in the development of such application (TataSteel) has also shown great interest in continuing pursuing its successful development. Although the experimental results are not yet available, they will become available after the timeframe of ATHOR.

2 Design of the 3D pilot steel ladle

As mentioned before, the first phase of this work is the design of the pilot. The scale of the pilot ladle should be such that the pilot ladle is big enough to represent the global behaviour of an industrial ladle and allow to install the measurement devices. However, it should also be small enough to be handled at the laboratory level. The other difficulties involved with the scale are the thickness of the steel shell and the size and shape of the refractory bricks. To tackle all these challenges, several simplified numerical campaigns were developed, assisting with the design and, ultimately, with the choices made regarding the installation itself.

Here, the objective was to assess different aspects of the pilot ladle, in such an order that it would be possible to make decisions on the final configuration of the installation throughout the design phase. Different aspects were tackled and described in the following sections:

- Definition of the overall dimensions (scale)
- Definition of the linings' thickness
- Definition of the steel shell thickness
- Definition of the pilot bottom
- Definition of the pilot height

2.1 Numerical modelling considerations

These simplified numerical simulations were performed in Abaqus [11]. These simulations aimed to observe the behaviour of an industrial steel ladle in terms of temperature, stress and strain distribution over the refractory linings. Similar simulations were performed at different scales. From such simulations, it was possible to observe the influence in the thermal and mechanical behaviour of the scaled ladles, of the size and shapes of the refractory bricks, etc. Following these observations, it was possible to converge on the pilot steel ladle scale. After the scale being decided, the next steps were to assess the steel shell, the top and bottom of the ladle.

2.1.1 Modelling approach

As the wear lining of the steel ladle is built with mortarless masonry, a simplified micro-modelling approach is adopted here. In this modelling approach, the spatial discretization of the masonry is performed at the level of brick elements, and the dry joints are represented by their contact behaviour using interface elements. Herein, brick elements are simulated with corresponding mechanical parameters of the material from which they are made, and their connection with contact elements that permit separation, penetration, and sliding at the contact. This modelling approach provides a detailed description of stress and strain

distribution and concentration in the bricks. For this numerical campaign only the temperature dependents elastic properties of the different materials were considered. Additional information regarding this approach is presented in Deliverable 3.6.

Bricks in the working lining are trapezoidal in shape. When modelled in its true shape, it creates an uneven gap between the wear lining and permanent lining. This difference can lead to stress concentration near the corners, and it can create convergence problem in the numerical analysis. Therefore, for simplicity, the back face of the wear lining is assumed to be curved to match the geometry of the subsequent permanent lining.

Due to the presence of the dry joints between the bricks, a free expansion joint of 0.2 mm was considered between the bricks in the wear and permanent linings. Due to the presence of a dry joint between the wear lining and permanent lining and compressibility of insulation, the dry joint between these linings was considered 3 mm Figure 2 (a). To model the expansion gap, low normal stiffness between the joints was considered as shown in Figure 2 (b) and (c). Initially, the shear was considered as a friction coefficient of 0.7 for all the joints. Also, thermal conductivity was considered infinite for all these interfaces regardless of the gap.

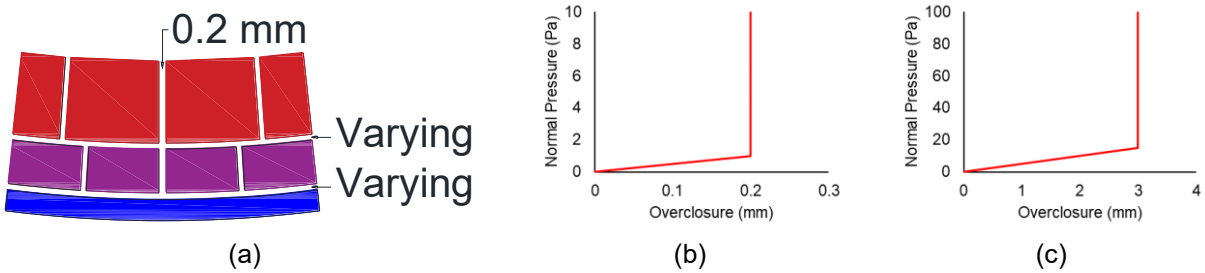

Figure 2 - Model considerations: a) schematic layout of joints; b) normal stiffness-overclosure profile for brick joints; c) normal stiffness-overclosure profile for expansion joints between the permanent lining and steel shell.

2.1.2 Material Properties

The thermomechanical properties for different lining materials were taken from the data shared by CRC, Tata Steel, Netherlands.

Mechanical properties of the wear linings are considered elastic with temperature dependency, as shown in Table 1 (Young's modulus is calculated by considering the linear behaviour between 30 % and 70 % of the peak stress). The wear lining density was considered 3200 kg/m^3, and Poisson's ratio was taken as 0.2. The temperature-dependent thermal conductivity of the wear lining is given in

Temperature [°C]	Young's Modulus [GPa]
20	36.94
800	33.34
1000	20.11
1200	18.36
1300	7.88
1400	3.23
1500	4.13

Table 2. A temperature-independent value of 7.8×10^{-6} K^{-1} has been taken for the thermal expansion coefficient α_{th}. The values of these material properties are comparable to the properties evaluated within the ATHOR project [12][13].

Table 1 - Mechanical properties of wear lining

Temperature [°C]	Young's Modulus [GPa]
20	36.94
800	33.34
1000	20.11
1200	18.36
1300	7.88
1400	3.23
1500	4.13

Table 2 - Thermal conductivity λ, and specific heat C_p (Wear lining)

T [°C]	50	250	500	750	1000
λ [W/m/K]	7.5	5.3	4.0	3.4	3.2
C_p [J/kg/K]	751	898	1104	1225	1250

European Commission
Horizon 2020
European Union funding
for Research & Innovation

The permanent lining and insulation layers are modelled as one effective layer for simplicity in analysis. **Error! Not a valid bookmark self-reference.** shows the harmonic average values for the stiffness and thermal conductivity of the effective insulation layer. A temperature-independent value has been taken for the thermal expansion coefficient $\alpha_{th} = 6.0\times10^{-6}$ K^{-1}, and C_p = 1200 J/kg/K. The effective mass density of this layer was taken as 2000 kg/m^3.

Table 3 - Young's modulus E and thermal conductivity λ of the effective refractory layer between wear lining and steel shell.

T [°C]	50	250	500	750	800	1000	1200	1250	1400
E [GPa]	1.8	-	-	-	1.8	1.6	1.4	-	0.6
λ [W/m/K]	0.50	0.52	0.58	0.65	-	0.73	-	0.81	-

Table 4 shows the mechanical and thermal properties of the steel shell considered in this analysis. The mass density of the steel shell is taken as 7850 kg/m^3.

Table 4 - Young's modulus E, thermal expansion coefficient α_{th}, thermal conductivity λ and specific heat C_p of the steel shell.

T [°C]	20	100	150	200	250	300	350
E [GPa]	192	191	189	186	183	179	173
αth [10^{-6}/K]	10.9	11.5	11.9	12.3	12.6	12.9	13.3
λ [W/m/K]	50	50	50	50	50	50	50
Cp [J/kg/K]	447	-	-	-	-	-	-

2.1.3 Boundary Conditions and loading

Symmetrical boundary conditions are applied to the ring model, as shown in Figure 3. This means that mirror symmetry is imposed on the edges with respect to the displacements, and there is no heat flux in the circumferential direction at the boundaries.

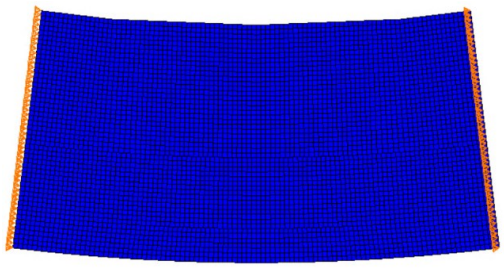

Figure 3 - Typical boundary conditions applied in the partial ring models

Regarding the thermal load, the following loading patterns are imposed (These conditions were derived from the thermal measurement data presented for an industrial steel ladle in *Deliverable D4.5: In-situ measurements on industrial steel ladle finished*):

- The initial temperature of 20 °C is applied to the whole assembly.
- The steel shell is exposed to a constant temperature of 20 °C with a heat transfer coefficient α of 9 W/m^2/K.
- Heating in 20 hours to 1050 °C with a heat transfer coefficient α of 300 W/m^2/K;
- Dwelling for 2 hours at 1050 °C with a heat transfer coefficient α of 300 W/m^2/K;
- 2.5 hours full-time with liquid steel of 1600 °C and heat transfer coefficient α of 500 W/m^2/K.

2.2 Definition of the overall dimensions (scale)

The first step into the design of the pilot ladle was the definition of the overall scale and dimensions of the installation. For this purpose, several aspects were considered, including the influence of different radius in the overall behaviour of the pilot, and the influence of the thickness of the different layers of the pilot. To assess these issues, different models were developed, analysed and described in the following sections.

2.2.1 Definition of the radius

To compare the thermomechanical behaviour of 3D laboratory scaled models with the industrial ladle, numerical simulations were carried out that considered various scaled models. Those results were compared with the result obtained for the industrial steel ladle. In this section, scaled models represent the reduction in the radius only. Thus, other geometrical parameters of the refractory bricks and steel shell have been kept the same as an industrial ladle. Here, for the wear lining, the total thickness taken was 140 mm, while to adjust for the reduced radii, the shape of the bricks in terms of inner dimension was changed, as shown in Figure 4. From this comparison, it will be possible to observe the effect of radius change on the overall behaviour of the reduced scaled steel ladles.

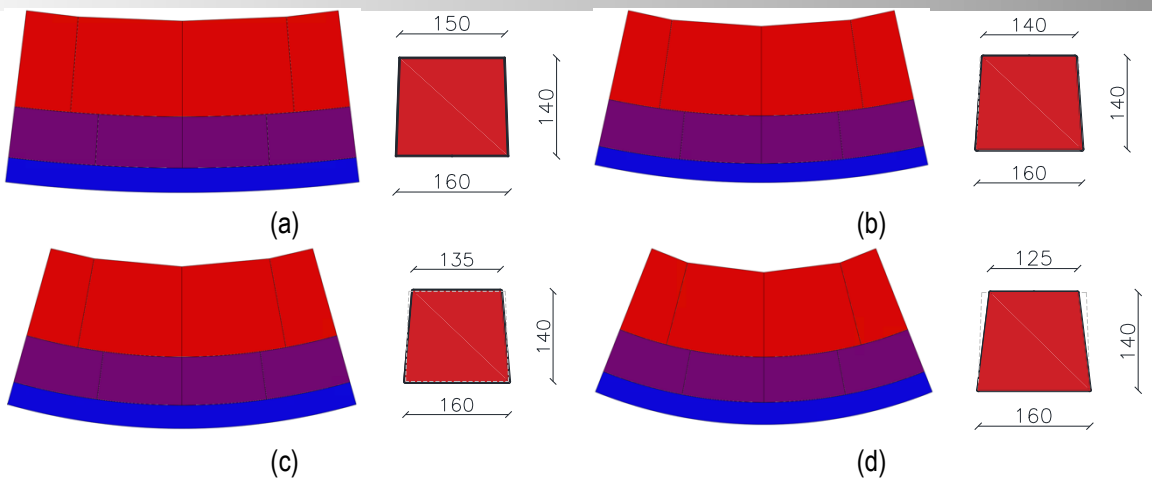

Figure 4 - Partial ring models with reduction in radius:
a) industrial scale (4.3m diameter); b) 2.45m diameter; c) 2m diameter; d) 1.5m diameter

Figure 5 shows the temperature distribution over the ring models at the end of the analysis (i.e. 24.5 hours). The results show that the temperature distribution over the body for all the cases is similar as the thermal properties and the lining thickness for all the models are identical. The temperature at the hot face was about 1580 °C and at the cold face was about 300 °C, which was expected from the adopted heat transfer coefficient.

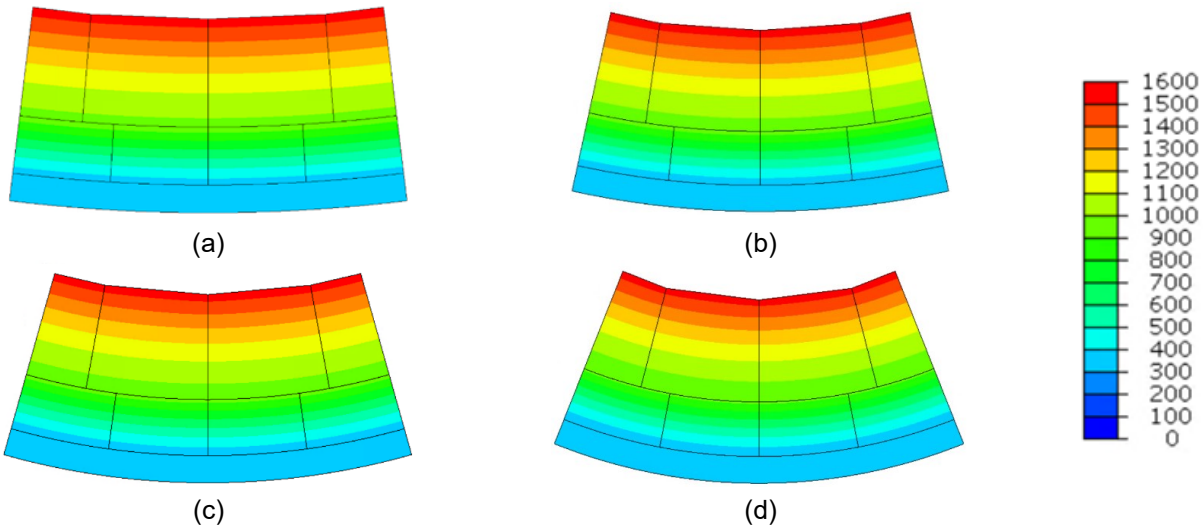

Figure 5 - Temperature distribution of the ring model [°C]:
a) industrial scale (4.3m diameter); b) 2.45m diameter; c) 2m diameter; d) 1.5m diameter

Figure 6 shows the distribution of circumferential stress in the wear linings of all partial ring models. Only circumferential stress distribution in the wear lining is shown for comparison purposes. From the figure, it is possible to observe that the maximum values of circumferential stress reduce with the reduction in the radius. It is also possible to observe that for the partial ring model with 2 m and 2.45 m diameter, most of the wear lining exhibits compressive stresses in the range of 7.5 MPa to 17.5 MPa, which is almost half than the stresses observed for the industrial ladle. For the partial ring model of 1.5 m diameter, it is possible to notice that wear lining exhibit almost null compressive stresses. Still, it exhibits some tensile stresses in the lower part of the linings. These differences are mainly due to the reduced radius of the steel ladle considered.

European Commission
Horizon 2020
European Union funding
for Research & Innovation

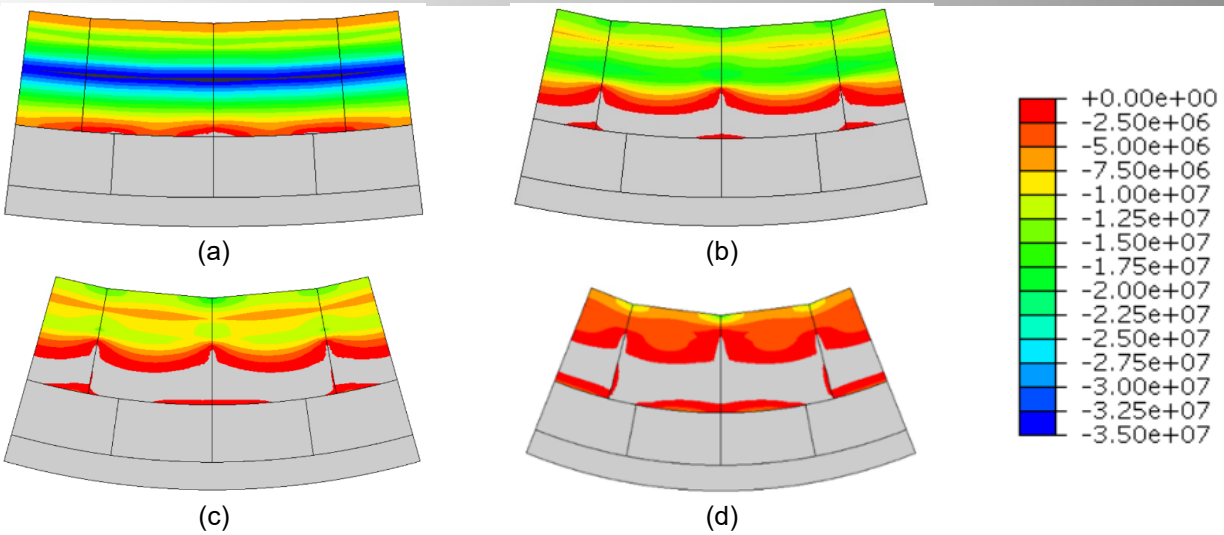

Figure 6 - Circumferential stress distribution [Pa]:
a) industrial scale (4.3m diameter); b) 2.45m diameter; c) 2m diameter; d) 1.5m diameter

The distribution of radial stress on the steel ladle and reduced scaled ladle is shown in Figure 7. From the results, it is possible to observe that for the radial direction, the partial ring models for the steel ladle exhibits a combined effect of tensile and compressive stress due to the internal thermal and mechanical boundary conditions implied by the thermal gradient and the dry joints within the refractory linings. From the results, stress concentrations can be noticed at the junctions between the bricks or linings, which are due to the difference of joint openings within the linings and between the bricks, due to the combined effects of thermal gradient and different thermal expansion coefficients of the refractory materials within the body. Moreover, it is possible to observe the high concentration of stresses near the brick joints for the reduced scaled models. Within the wear linings, these are due to the high restraint provided by the steel shell, which prevents movement of bricks and thus exhibits high constrains in the brick linings, which results in increased stress concentrations.

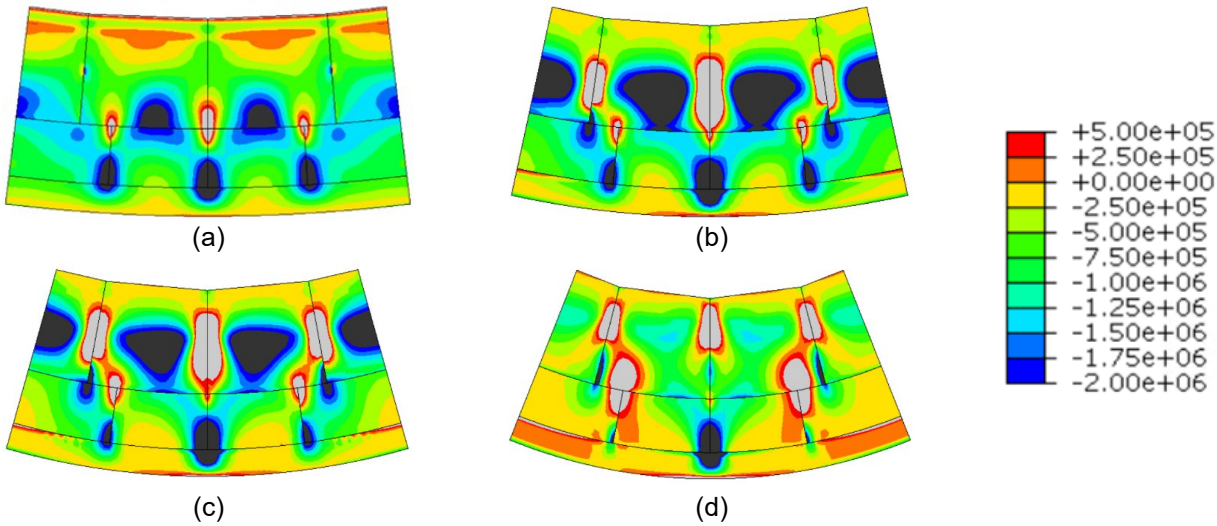

Figure 7 - Radial stress distribution [Pa]: a) industrial scale (4.3m diameter); b) 2.45m diameter; c) 2m diameter; d) 1.5m diameter

To evaluate the overall behaviour of the steel shell, Von Mises stress distribution for all the models is shown in Figure 8. From these results, it is possible to observe that in the case of an industrial steel ladle, circumferential stresses are in the range of 70 MPa, while for the reduced scaled models, this value decreases. This is due to the fact that for the reduced scale models, the steel shell exhibits a low level of circumferential stresses due to the reduced diameter and also due to the high thickness of the steel shell considered for these scaled models.

European Commission
Horizon 2020
European Union funding
for Research & Innovation

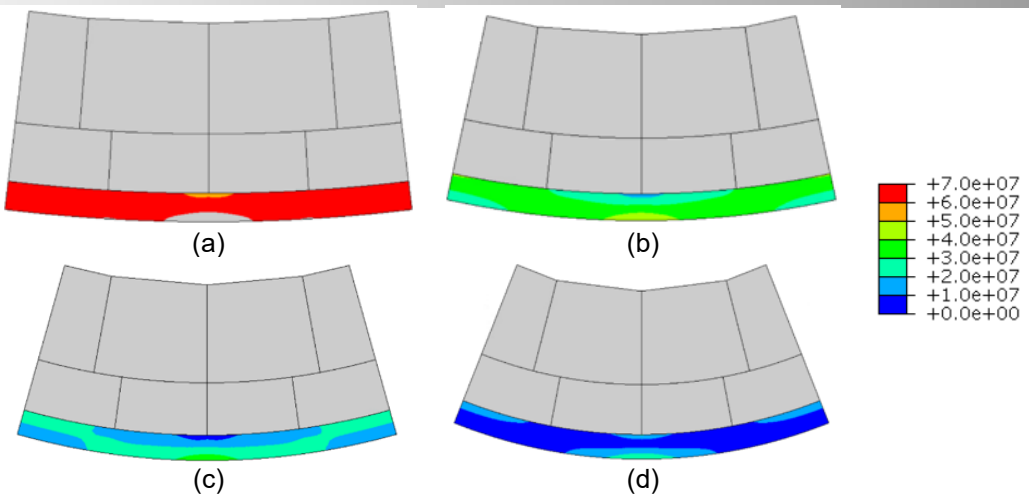

Figure 8 - Von Mises stress distribution [Pa]:
a) industrial scale (4.3m diameter); b) 2.45m diameter; c) 2m diameter; d) 1.5m diameter

From the analyses performed for the reduced scaled models considering the same thicknesses of all the linings, it is possible to observe that due to the same thicknesses of the linings and same thermomechanical properties, the temperature distribution of reduced scaled ladles is similar to the industrial steel ladle. It is also possible to observe that the steel shell provides a high level of constraints on the refractory lining. Because of that, refractory linings show a low level of circumferential stresses and higher radial stresses. The steel shell itself exhibits low circumferential stresses, suggesting that the steel shell is underutilised in these cases. The combinations of these differences compared to the industrial steel ladle approaches keeping the same thickness for the reduced scaled ladles diverge from the aim of having similar behaviour as the industrial ladle.

2.2.2 Model with scaled thickness

Due to the differences observed in the approach taken in section **Error! Reference source not found.**, in this section, the reduced scaled models for the 3D pilot steel ladle designs are considering the reduction in the thicknesses of the linings as well. The reductions are applied in proportion to the reduced diameter of the steel ladle, as shown in Figure 9. The scaling is only made in the wear linings and steel shell as it was assumed that reducing the safety linings would lead to a much higher temperature on the steel shell. The thicknesses taken in these models are shown in Table 5. From these simulations, it will be possible to observe the effect of the reduction of lining thickness on the overall behaviour of the scaled steel ladles.

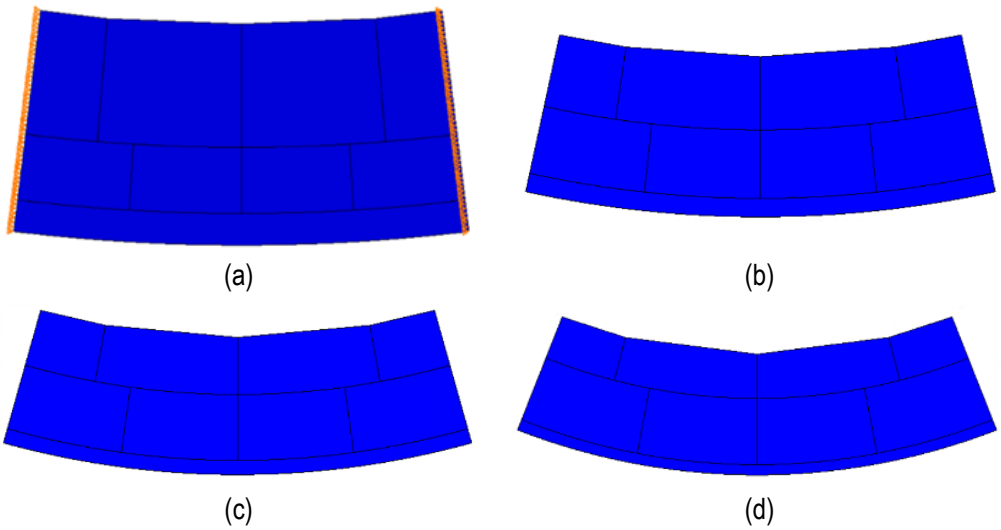

Figure 9 - Partial ring models with a reduction in radius and thickness:
a) industrial scale (4.3m diameter); b) 2.45m diameter; c) 2m diameter; d) 1.5m diameter.

European Commission
Horizon 2020
European Union funding
for Research & Innovation

Table 5 - Reduced thicknesses considered of different models

Model	Wear lining (mm)	Steel shell (mm)
Industrial scale	140	36
2.45 m diameter	80	20.5
2 m diameter	65	16.75
1.5 m diameter	50	12.5

Figure 10 shows the temperature distribution for the ring models at the end of the analysis (i.e. 24.5 hours). From the results, it is possible to observe that the temperature distribution over the body for all the cases exhibits high differences compared to the industrial steel ladle, due to the change of thickness in the wear lining. The maximum temperature observed for these models (steel shell) was 460 °C, 500 °C and 550 °C for models with 2.45m, 2m and 1.5m diameter, respectively.

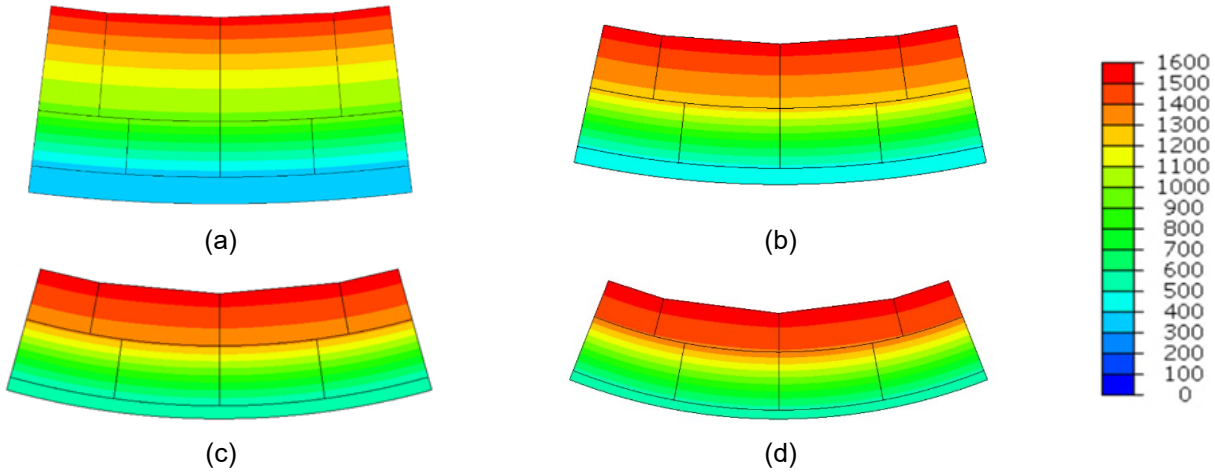

Figure 10 - Temperature distribution of the ring model [°C]:
a) industrial scale (4.3m diameter); b) 2.45m diameter; c) 2m diameter; d) 1.5m diameter

Figure 11 shows the circumferential stress distribution in the wear linings of all partial ring models. Only circumferential stress distribution in the wear lining is shown for comparison purposes. From the figure, it is possible to observe that the maximum values of circumferential stress decreases with the reduction in the radius and the thickness of the wear linings. Results for the 2 m and 1.5 m diameter shows that the circumferential stresses in the wear lining are close to null. This is due to the similar range of temperature distribution in the wear lining (as opposed to the industrial model where a temperature gradient is evident) as well as the reduced radius of the ladle. While for the model with a 2.45 m diameter, it is possible to observe the compressive stresses in the outer side.

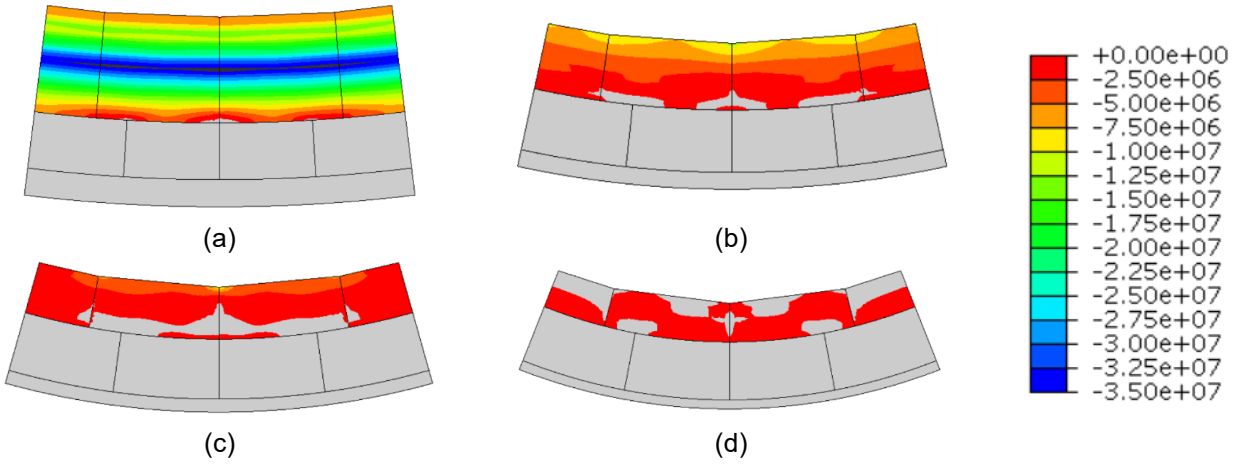

Figure 11 - Circumferential stress distribution [Pa]:
a) industrial scale (4.3m diameter); b) 2.45m diameter; c) 2m diameter; d) 1.5m diameter

The distribution of radial stress on the steel ladle and scaled ladles is shown in Figure 12. From the results, it is possible to observe that for the reduced thickness models with 2.45m, radial stresses are in a similar range to that of the industrial ladle.

European Commission | Horizon 2020 European Union funding for Research & Innovation

However, with the decrease in the diameters (i.e. 2m and 1.5m), it can be observed that due to the small thickness of the wear linings and constant temperature distribution in the wear linings, the linings exhibit a lower level of stress.

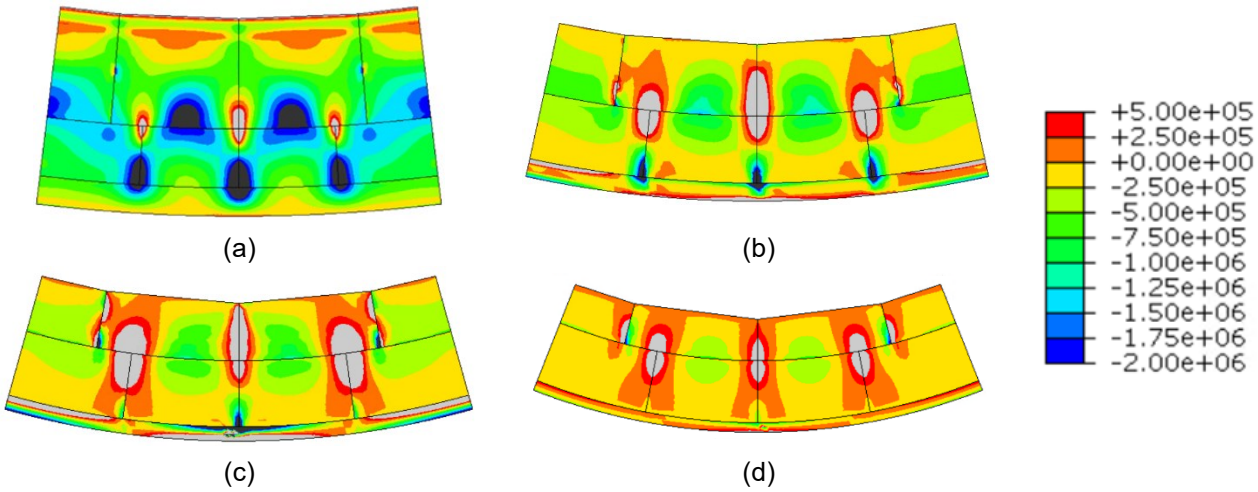

Figure 12 - Radial stress distribution [Pa]:
a) industrial scale (4.3m diameter); b) 2.45m diameter; c) 2m diameter; d) 1.5m diameter

To evaluate the overall behaviour of the steel shell, Von Mises stress distribution for all the models is shown in Figure 13. From these results, it is possible to observe that in the case of an industrial steel ladle, circumferential stresses are in the range of 70 MPa. At the same time, for the scaled models, these values are lower than those observed in section **Error! Reference source not found.**, where the steel shell thickness was higher than in this case. This decrease in stresses in the steel shells of the scaled ladles can be explained by the decrease in the pressure applied by the wear linings on the steel shell due its reduced thickness.

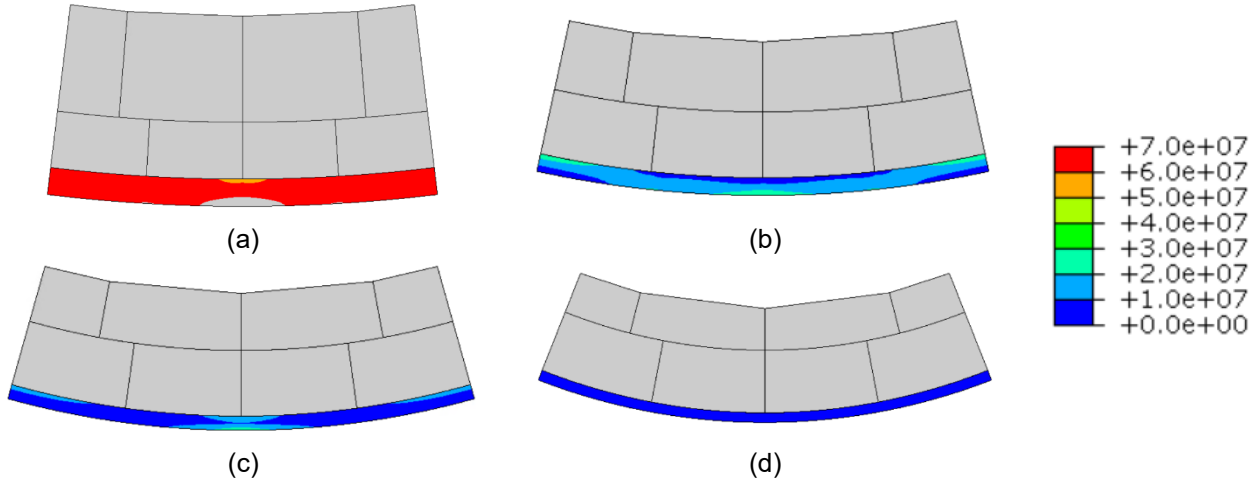

Figure 13 - Von Mises stress distribution [Pa]:
a) industrial scale (4.3m diameter); b) 2.45m diameter; c) 2m diameter; d) 1.5m diameter

From the analyses performed on the scaled models considering different thicknesses for all the linings, it is possible to observe that due to the different thicknesses of the linings, the temperature observed in the steel shell was much higher compared to the industrial steel ladle. These high temperatures in the steel shell can be unsafe for the laboratory environment and hinder data acquisition systems such as strain gauges. Also, it was observed that the reduction in the thickness of the wear linings does not show similar thermomechanical behaviour as an industrial steel ladle. This is due to the similar range of high temperature observed within the wear linings for these cases, which do not generate internal thermal restrains required for the generation of high stresses.

2.2.3 Model with mixed thickness

As observed in sections **Error! Reference source not found.** and **Error! Reference source not found.**, just a reduction in the radius of the pilot or even a proportional decrease in the thickness, does not correspond to exhibiting a behaviour similar to that of an industrial steel ladle. To overcome this problem, in this section, models with combined thickness, i.e. the same thickness of wear lining as industrial ladle and reduced steel shell (Table 6) thickness, are analysed as shown in Figure 14.

European Commission | Horizon 2020 European Union funding for Research & Innovation

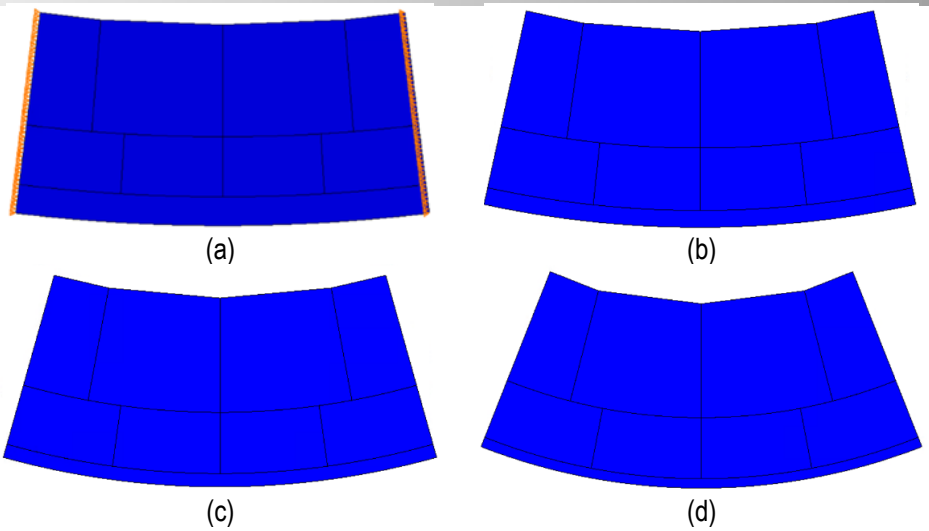

Figure 14 - Partial ring models with a reduction in radius and steel shell thickness: a) industrial scale (4.3m diameter); b) 2.45m diameter; c) 2m diameter; d) 1.5m diameter

Table 6 - Reduced thicknesses considered of different models

Model	Wear lining (mm)	Steel shell (mm)
Industrial scale	140	36
2.45 m diameter	140	20.5
2 m diameter	140	16.75
1.5 m diameter	140	12.5

Figure 15 shows the temperature distribution over the ring models at the end of the analysis (i.e. 24.5 hours). From the results, it is possible to observe that the temperature distribution over the body for all the cases exhibits close temperature distribution as in the case of an industrial steel ladle. This is due to the same thickness of wear lining considered in the scaled models. However, it was observed that, because the thickness of the steel shell is reduced, the temperature in the steel shell is 350°C (higher than the case of industrial steel ladle with 300°C).

Figure 16 shows the circumferential stress distribution in the wear linings of all partial ring models. From the figure, it is possible to observe that the range of stresses observed in the scaled models are similar to those observed in section **Error! Reference source not found.**, which shows that the magnitude of circumferential stresses depends on the radius of the scaled model. As the radius decreases, the circumferential stresses also decreases.

The distribution of radial stress on the steel ladle and scaled ladles is shown in Figure 17. From the results, it is possible to observe that the range of the stresses observed in the wear linings is similar to that observed in section **Error! Reference source not found.**. But the intensity of maximum stresses observed in this case is lower when compared to that of section **Error! Reference source not found.**. This shows that the radial stress distribution depends on the thickness of the wear lining and the thickness of the steel shell.

European Commission
Horizon 2020
European Union funding
for Research & Innovation

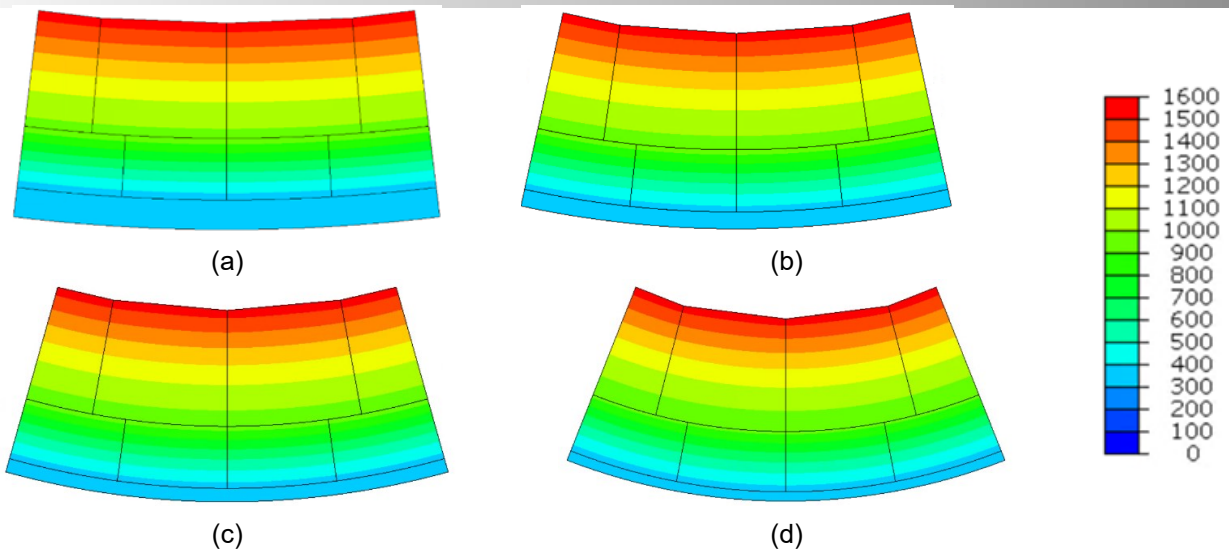

Figure 15 - Temperature distribution of the ring model [°C]:
a) industrial scale (4.3m diameter); b) 2.45m diameter; c) 2m diameter; d) 1.5m diameter

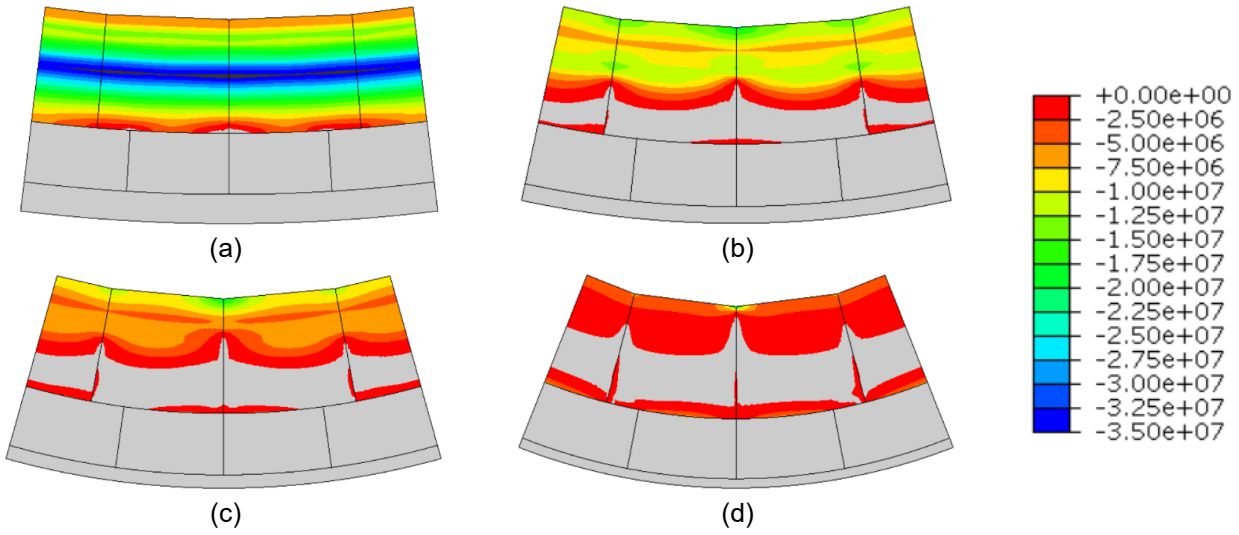

Figure 16 - Circumferential stress distribution [Pa]:
a) industrial scale (4.3m diameter); b) 2.45m diameter; c) 2m diameter; d) 1.5m diameter

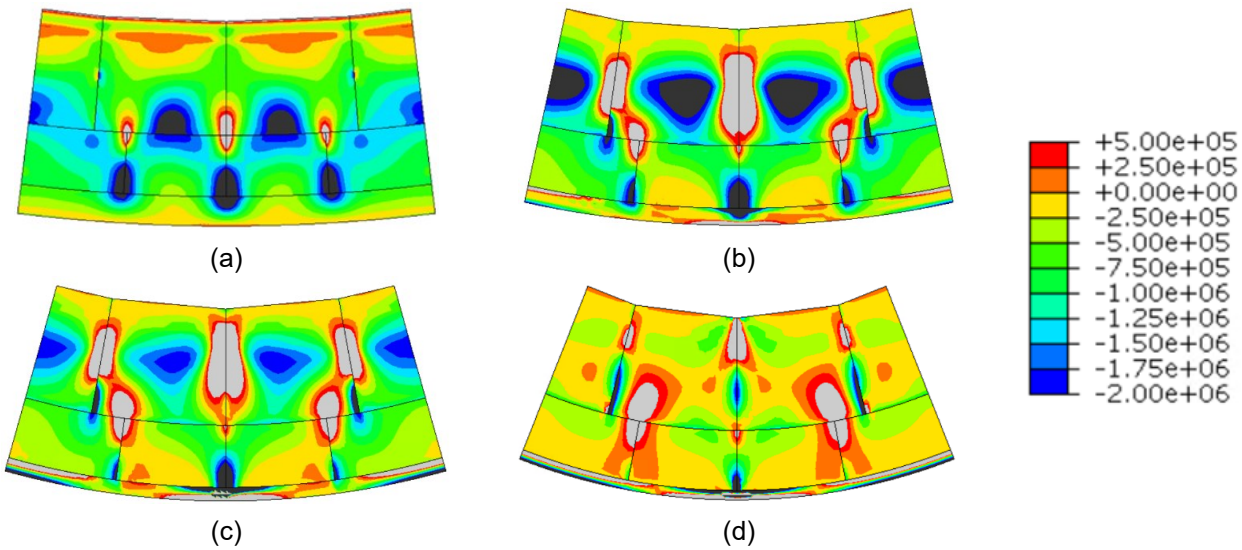

Figure 17 - Radial stress distribution [Pa]: a) industrial scale (4.3m diameter); b) 2.45m diameter; c) 2m diameter; d) 1.5m diameter

European Commission
Horizon 2020
European Union funding
for Research & Innovation

To evaluate the overall behaviour of the steel shell, Von Mises stress distribution for all the models is shown in Figure 18. From these results, it is possible to observe that in the case of an industrial steel ladle, circumferential stresses are in the range of 70 MPa. At the same time, for the scaled models, these values are higher than the ones observed in section **Error! Reference source not found.**, where the steel shell was thicker. This shows that for the same configuration of the refractory linings, circumferential stresses in the steel shell increases with the reduction in the steel shell thickness, which was expected.

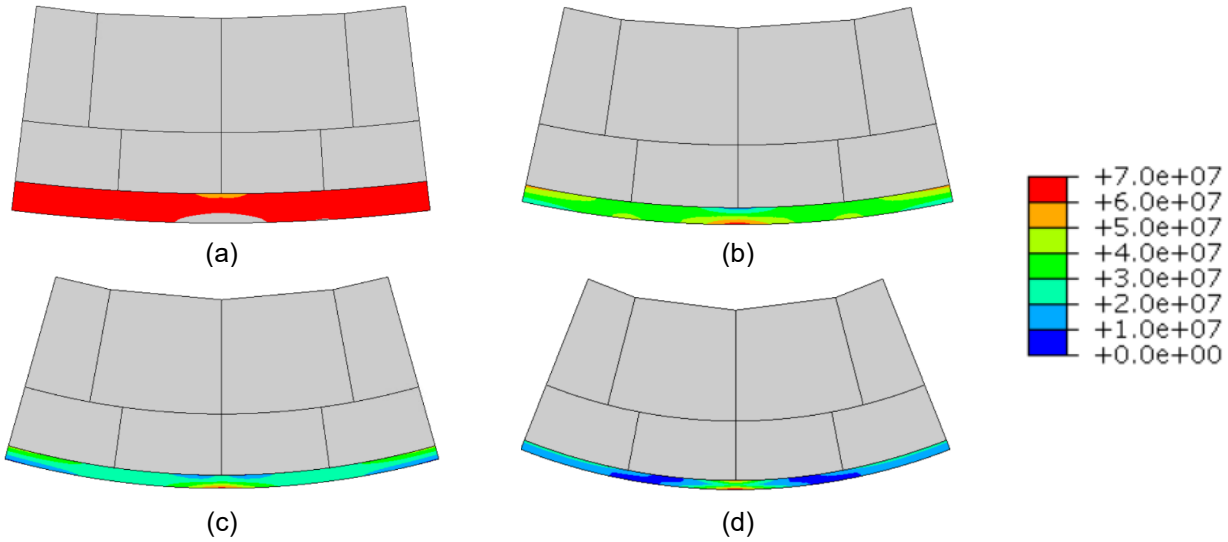

Figure 18 - Von Mises stress distribution [Pa]:
a) industrial scale (4.3m diameter); b) 2.45m diameter; c) 2m diameter; d) 1.5m diameter

From the analyses performed on the scaled models considering combinations of the thicknesses, it is possible to observe that these shows better overall results when compared to the approaches described in sections **Error! Reference source not found.** and **Error! Reference source not found.**. This approach (combined thickness into a reduced scale) seems to show better performance when considering the manufacturing and building of a scaled model of a steel ladle. As per the simulation results and space availability, it was decided to build a pilot ladle with a 1.5 m diameter. From the analyses performed in this section, it can be observed that the adopted steel thicknesses in various models do not exhibit the same stress ranges in steel shell compared to the industrial ladle, which shows that further simulations with varying steel shell thicknesses are required to converge to a solution which offers close behaviour as an industrial ladle.

2.3 Optimisation of steel shell thickness

For optimisation, different thicknesses of steel shells were considered for the pilot ladle of 1.5 m diameter. In the previous report for the pilot ladle of this scale, the thickness considered was 12.5 mm, which was a proportional reduction from an industrial scale (4.3 m diameter) to the reduced scale (1.5 m diameter). But this thickness of steel plate is not available widely for commercial purposes. Considering the commercial availability of steel plates, different thicknesses of steel shells of pilot ladle were studied, namely: 6, 8, 10, 12, 13, 14, and 16 mm.

In the optimisation process, the prime focus was given to the stresses presented on the steel shell and its capability to resist the same. But it was also considered interesting to see the effect of steel shell thickness on the overall thermomechanical behaviour of the pilot ladle linings. In Figure 19, the temperature distribution in the linings for 6, 12.5 and 16 mm of steel shell thicknesses, is presented.

European Commission
Horizon 2020
European Union funding
for Research & Innovation

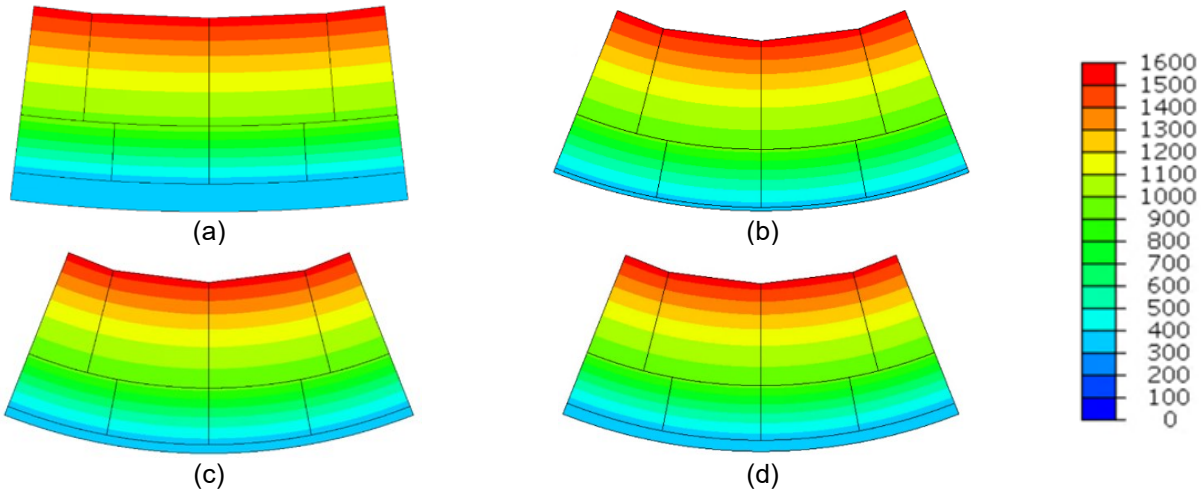

Figure 19 - Temperature distribution of the ring model [°C]:
a) industrial scale (4.3m diameter); b) 6mm steel shell; c) 12.5mm steel shell; d) 16mm steel shell

From the results, it can be observed (considering both extremes of values under study) that the reduction or increase of steel shell thickness does not impact the temperature distribution in the steel shell or other linings to a great extent, as these variations (in shell thickness) are marginal compared to the overall thickness of the linings of the ladle.

Figure 20 shows the distribution of circumferential stress in the wear linings of the industrial scale ladle (4.3m diameter) and scaled models with 6, 12.5 and 16 mm thickness. The results show that even though the distribution of stresses is not similar to an industrial ladle due to the size effect, the distribution of these stresses does not vary significantly when the steel shell thickness is changed. Similarly, the distribution of radial stress on the steel ladle and reduced scaled ladle is shown in Figure 21. From the results, it is possible to observe that the choice of different steel shell thicknesses does not impact the overall behaviour of different linings of the pilot ladle.

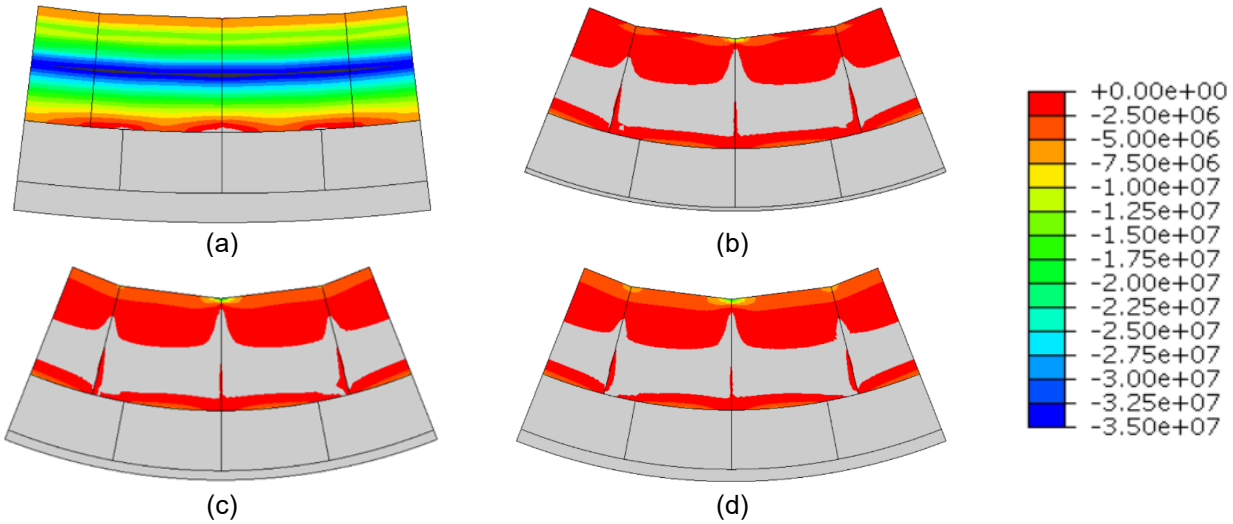

Figure 20 - Circumferential stress distribution [Pa]:
a) industrial scale (4.3m diameter); b) 6mm steel shell; c) 12.5mm steel shell; d) 16mm steel shell

European Commission
Horizon 2020
European Union funding
for Research & Innovation

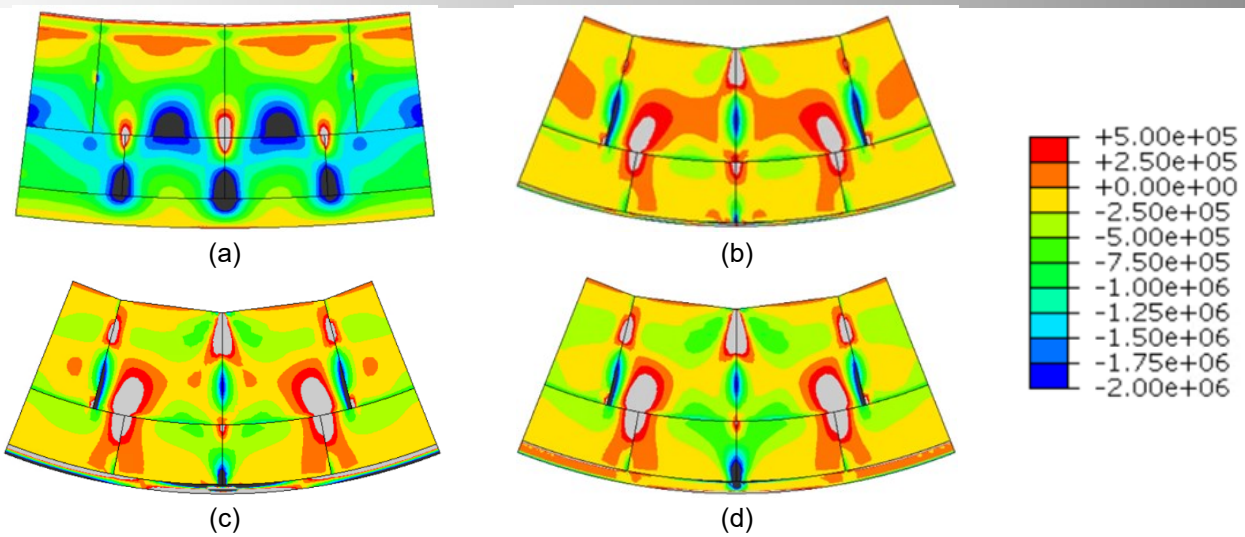

Figure 21 - Radial stress distribution [Pa]:
a) industrial scale (4.3m diameter); b) 6mm steel shell; c) 12.5mm steel shell; d) 16mm steel shell

From these previous comparisons (of temperature distributions; and stress distributions at the lining layers), considering both extreme values for the shell thickness, it can be concluded that the choice of steel shell thickness will not alter the overall behaviour of the linings of the pilot ladle, therefore, to choose an optimum thickness of the steel shell only the distribution of stresses in the steel shell should be considered.

Figure 22 presents the distribution of the Von Mises stresses that can be observed when considered with the different thicknesses of the steel shell. The results show that the distribution and magnitude of the stresses in the steel shell do not change, keeping the same areas with stress concentration and with similar peak values. This is because of the low level of pressure the steel shell experiences, considering the lower diameter of the ladle. However, stress concentrations can be observed near the locations where dry joints are considered in the refractory linings due to joint behaviour. It can also be observed that, as the steel shell thickness decreases, the number of stress concentration zones also decreases. From the results, a ladle with a steel shell of 6mm thickness seems like an optimum solution, but further discussions are needed to confirm this (section 2.6). The average stress observed in that steel shell was 15 MPa, and the highest stress was 80 MPa in the same steel shell near the dry joints.

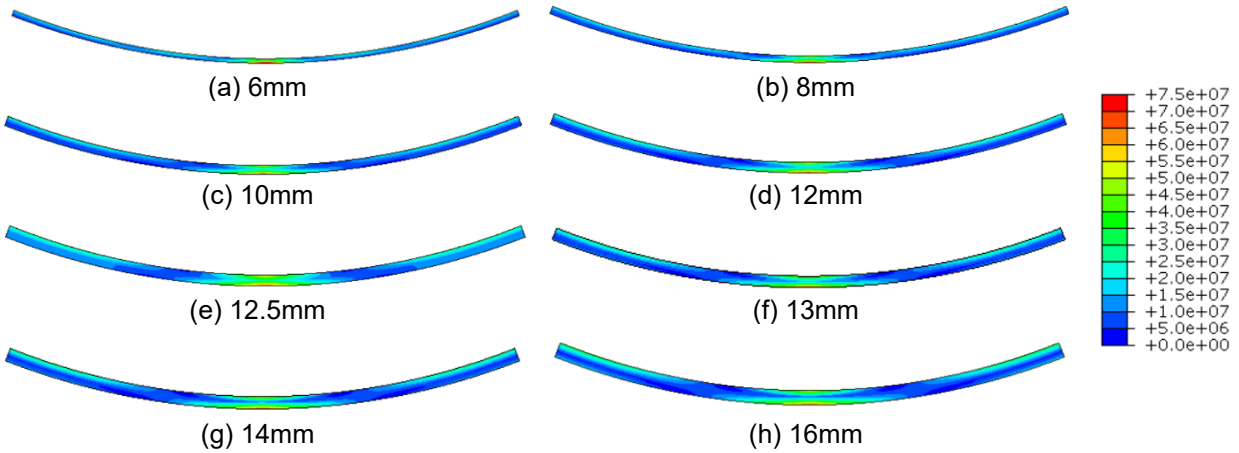

Figure 22 – Von Mises stress distribution in steel shell with different thicknesses

From the optimisation of steel shell thickness for the 1.5m diameter pilot steel ladle, it was observed that with the small variations in the thickness of the steel shell, overall thermal and mechanical behaviour does not vary significantly. The analyses also found that a pilot ladle of 1.5m diameter with 6mm steel shell thickness seems safe to use.

2.4 Influence of steel ladle bottom

To observe the influence of the steel shell bottom on the overall behaviour of the ladle, analyses were performed on a 3D quarter model with and without bottom for a 1.5m diameter steel ladle with 6mm steel shell thickness. In these simulations, dry joints between the bricks in a same lining were not considered, and all the joints within a lining were assumed to be closed to reduce the computational time. Both models will yield a high amount of stress, but it was deemed suited for comparison purposes.

European Commission | Horizon 2020 European Union funding for Research & Innovation

However, joints between the different linings were considered the same as in partial ring models. Also, apart from loads and symmetrical boundary conditions considered in the partial ring model, gravity loads due to self-weight and only vertical supports at the bottom of the ladle were considered (Figure 23).

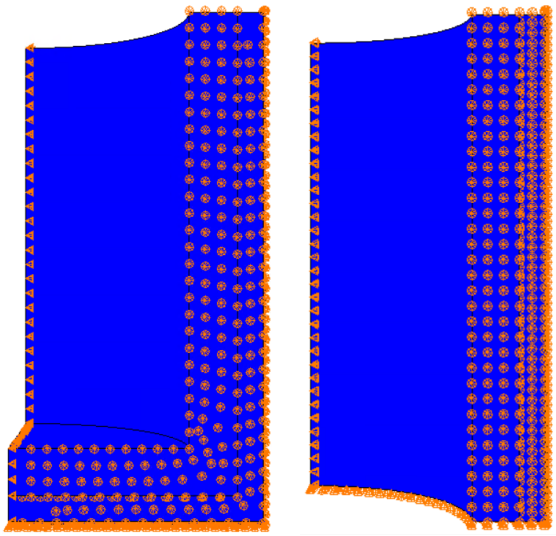

(a) (b)

Figure 23 - 3D quarter models of 1.5m diameter pilot steel ladle: a) with ladle bottom; b) without ladle bottom

Figure 24 shows the distribution of temperature in these models. From the analysis, it can be observed that the temperature distribution in the steel ladle wall does not exhibit significant difference due to the presence of ladle bottom except for the location near the junction of ladle wall and the bottom (corner).

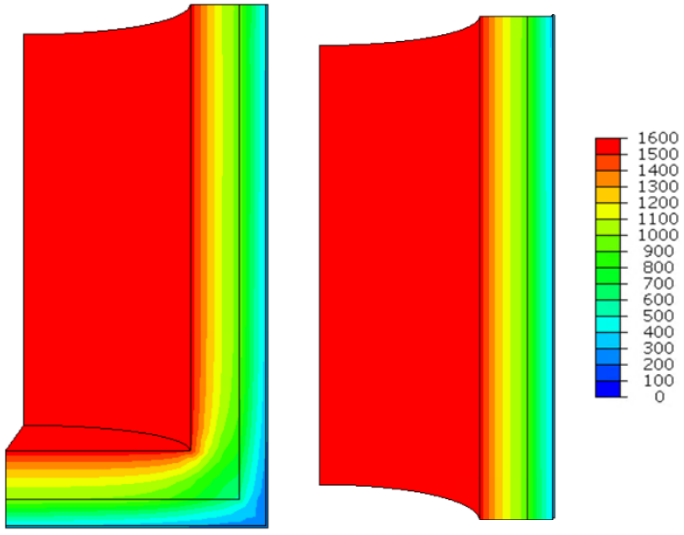

(a) (b)

Figure 24 - Temperature distribution of the quarter model [°C]: a) with ladle bottom; b) without ladle bottom

Figure 25 shows the distribution of circumferential stress in the model. The results show that the distribution (and magnitude) of these stresses within the wall and the linings are similar in both cases. From both models, it can be observed that the stresses at the top of the ladle (in the wear linings) are lower due to the free vertical expansion of the wear lining at that location for both cases. However, the influence due to the ladle bottom can be observed at the bottom of the wear lining. This difference (between both models) is not prominent in terms of the overall effect, but some stress concentrations can be observed in the wear linings closer to the junction of the wall and bottom of the ladle. This stress concentration can be decreased if all the dry joints between the bricks are considered. Still, no significant influence of the ladle bottom can be found in the wear lining in terms of its overall circumferential behaviour.

European Commission
Horizon 2020
European Union funding
for Research & Innovation

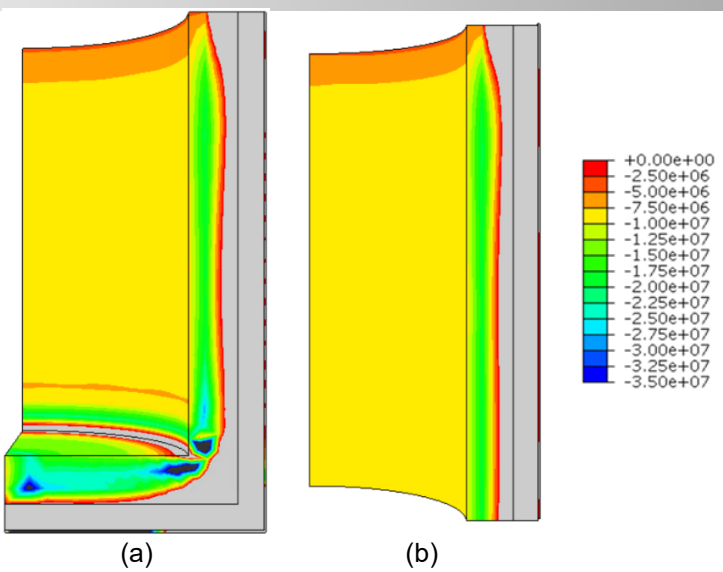

Figure 25 - Circumferential stress distribution [Pa]: a) with ladle bottom; b) without ladle bottom

The distribution of radial stresses in the quarter models is shown in Figure 26. The results show that due to the free vertical expansion of wear linings at the top of the wall, stresses are compressive. In the case of the ladle with the bottom, a difference in the distribution of stresses can be observed. The ladle bottom causes the higher compressive radial stress in the ladle bottom and wall junction, but the effect of the ladle bottom seems to be reducing on the central and upper part of the ladle wall. From the distribution of radial stresses, it can be observed that the influence of the ladle bottom on the radial behaviour of the wall is not negligible but limited to the lower section of the wall.

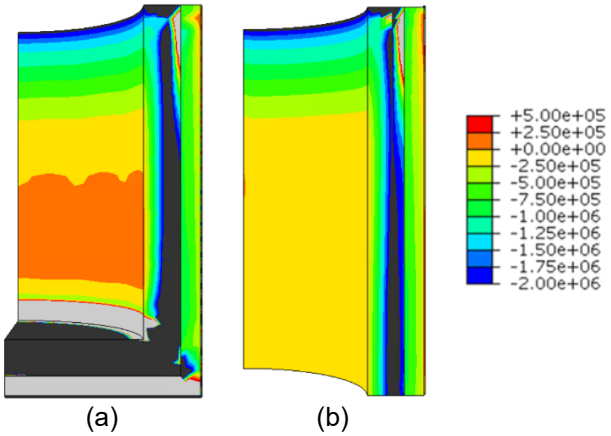

Figure 26 - Radial stress distribution [Pa]: a) with ladle bottom; b) without ladle bottom

Figure 27 shows the distribution of the Von Mises stresses in the steel shell of the pilot steel ladle for both cases. From the results considering the model with ladle bottom, it can be observed that due to the restraining effect of the ladle bottom on the ladle wall, stresses in the ladle bottom are higher (up to 200 MPa) and, because of this restraining effect, stresses in the bottom part of the ladle wall are higher, which reduces to 0.1 MPa at the top. In the case of ladle without bottom, it can be observed that the lower and central part of the wall exhibit tensile stresses in the magnitude of 0.1 MPa while the stresses at the top are higher due to the free expansion of the wear lining at the top. This effect (free expansion at the top) was also observed in the case with ladle bottom, but high-stress distribution was not observed due to the restraining influence of ladle bottom.

European Commission
Horizon 2020
European Union funding
for Research & Innovation

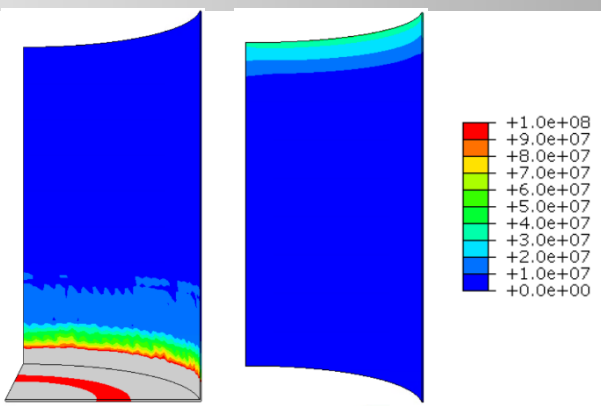

Figure 27 – Von Mises stress distribution [Pa]: a) with ladle bottom; b) without ladle bottom

Comparison of the 3D quarter models with and without the ladle bottom shows that the presence of the ladle bottom influences the radial behaviour of the wear linings significantly but is limited to the bottom section. Also, the distribution of the Von Mises stresses varies significantly when the ladle is considered with or without the steel ladle bottom. Both models seem to be helpful for the thermomechanical characterisation of the ladle with their own merits and drawbacks. The model with a ladle bottom will help to characterise an industrial ladle's global behaviour (including cornering effects). In contrast, a model without a ladle bottom will help describe the refractory lining behaviour in a steel ladle (without cornering effects, analysing only the barrel). Therefore, it was decided to opt for the pilot ladle without a ladle bottom, which will provide insight into the behaviour of the wear lining and its influence on the barrel of the ladle.

2.5 Influence of the height of ladle

To assess the influence of the height of the ladle wall on the behaviour of the ladle, 3D quarter model of 1.5 m diameter ladle with 6 mm thickness of steel shell was considered with 300 mm (3 bricks), 500 mm (5 bricks) and 1000 mm (10 bricks) height of the ladle wall (Figure 28). This model was analysed without the ladle bottom. As the objective of this analysis was to assess the influence of the height, dry joints between the joints of the wear linings were considered only in the vertical direction (i.e. bed joints of 0.2 mm initial gap). No joints were considered for the head joints, resulting in higher circumferential stress, but this comparison of the height effect was deemed fit. Material properties, loads and symmetrical boundary conditions were the same as the partial ring models. Still, the self-weight and the vertical support at the bottom of the ladle were also considered.

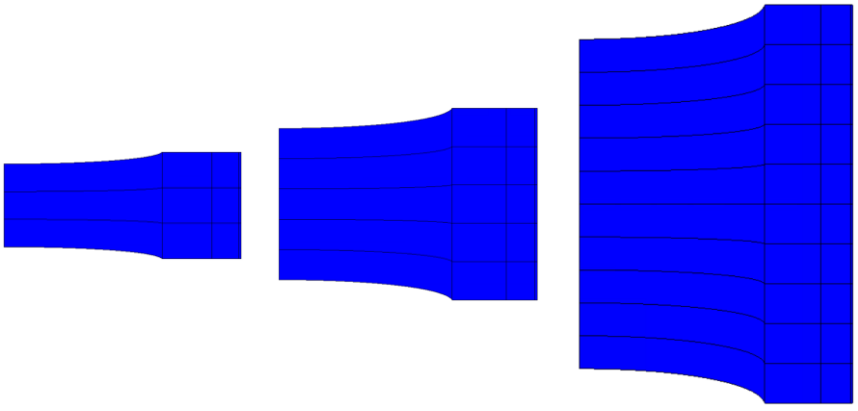

Figure 28 - 3D quarter model of pilot steel ladle of 1.5m diameter: a) 3 bricks; b) 5 bricks; c) 10 bricks

Figure 29 shows the temperature distribution in the 3D quarter model of the pilot ladle with 1.5m diameter for the 3 cases considered (3 bricks, 5 bricks and 10 bricks). For the cases considered, the temperature distribution within the structure does not change as the top and bottom part of the ladle is deemed adiabatic.

European Commission | Horizon 2020 European Union funding for Research & Innovation

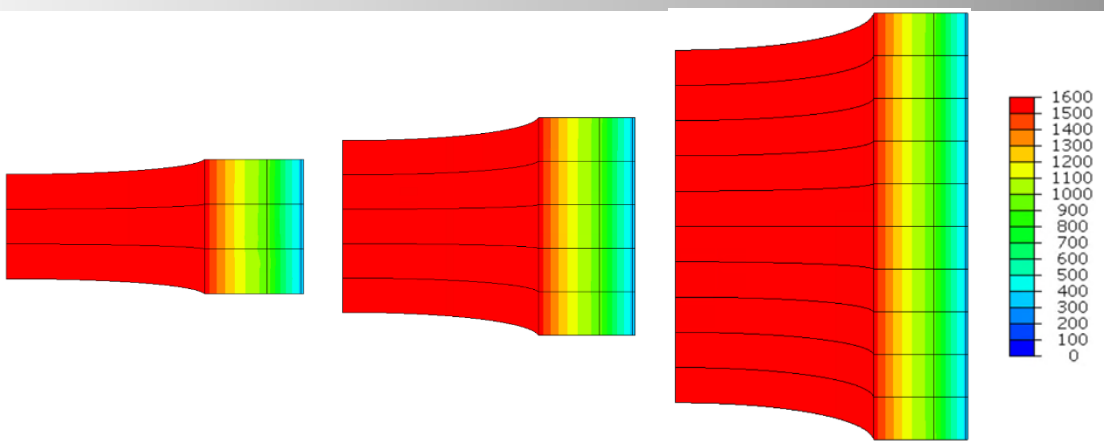

Figure 29 - Temperature distribution in the quarter model [°C]: a) 3 bricks; b) 5 bricks; c) 10 bricks

Figure 30 shows the distribution of the circumferential stresses in the 3D quarter models. From the results, it is possible to observe that due to free vertical expansion of the bricks in the top layer, stresses observed in that layers are smaller compared to other layers, while for all the models bottom layer shows high circumferential stress distribution, this may be due to the gravity loads of all the bricks and vertical support conditions.

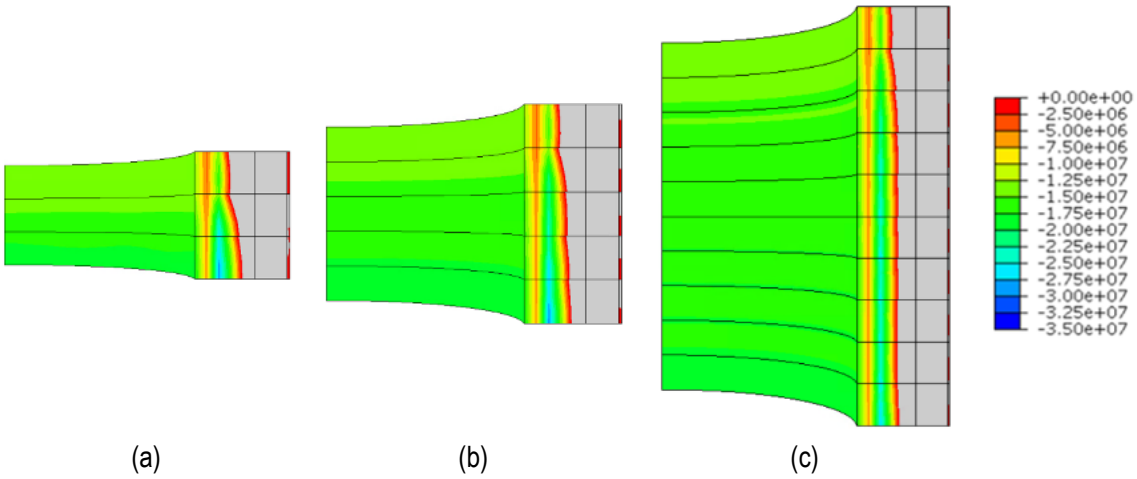

Figure 30 – Circumferential stress distribution [Pa]: a) 3 bricks; b) 5 bricks; c) 10 bricks

The distribution of radial stresses for the 3D quarter models is shown in Figure 31. From the results, it is possible to observe that for all the models considered, the radial distribution of stress exhibits a non-regular pattern due to internal thermal and mechanical (mainly bed joints) constraints. Moreover, it is possible to observe that the top 2 layers of bricks show different behaviour for all the cases compared to the lower levels of bricks. This may be due to gravity and support considerations.

European Commission
Horizon 2020
European Union funding
for Research & Innovation

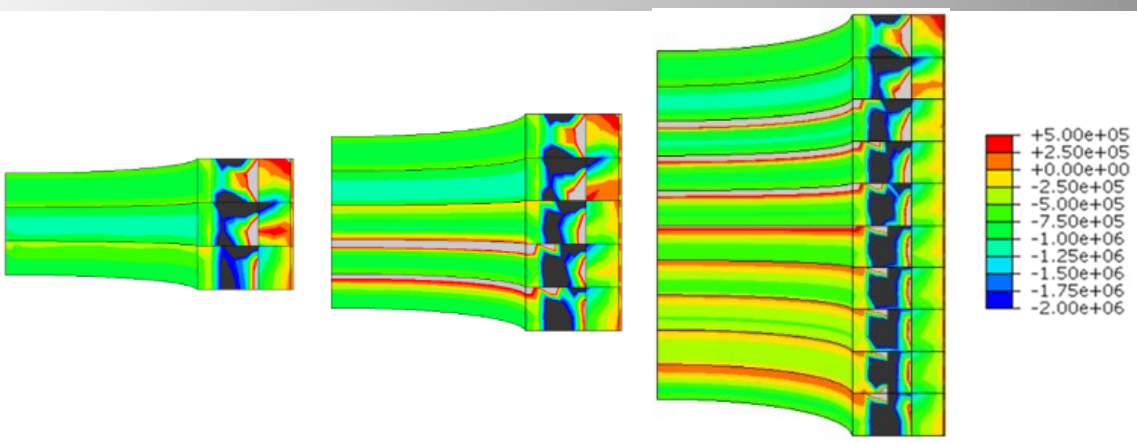

(a) (b) (c)

Figure 31 - Radial stress distribution [Pa]: a) 3 bricks; b) 5 bricks; c) 10 bricks

Figure 32 shows the Von Mises stresses distribution in the ladle's steel shell for all cases. From the results, it is possible to observe that the stress distribution is irregular for the ladles with a low height. In contrast, for the model with 10 bricks, the distribution of stresses gets normalised after the first 3 layers of bricks.

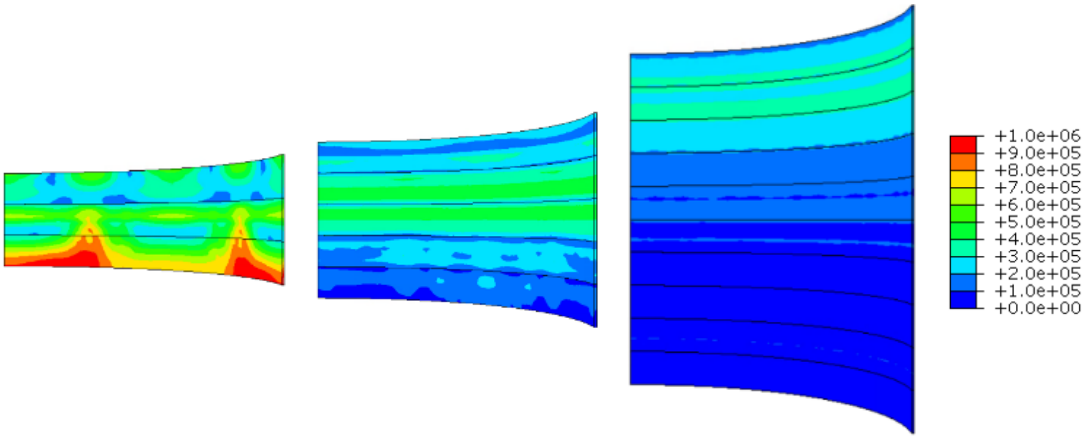

(a) (b) (c)

Figure 32 – Von Mises stress distribution [Pa]: a) 3 bricks; b) 5 bricks; c) 10 bricks

From the analyses performed on 3D quarter models with different heights, it was observed that the stress distribution is not regular for the ladles with lower height (i.e. 300 mm) due to the influence of free expansion at top and bottom vertical support. A pilot ladle with 500 mm height (i.e. with 5 bricks) was deemed sufficient to counter these effects. The measurements performed at the central part of this ladle will acquire results that will not be influenced by the thermal and mechanical constraints at the top and bottom.

2.6 Capacity analysis of the steel shell

To assess the performance of the steel shell (6 mm thickness and 500 mm height), nonlinear analyses were carried out. The steel shell should behave within its elastic limits during the lifetime of the installation. For this purpose, two analyses were performed. The first analysis focuses on the gravity loading due to self-weight and partial loads from the top insulation. Simplified nonlinear properties considered for the steel shell is shown in Figure 33.

European Commission | Horizon 2020 European Union funding for Research & Innovation

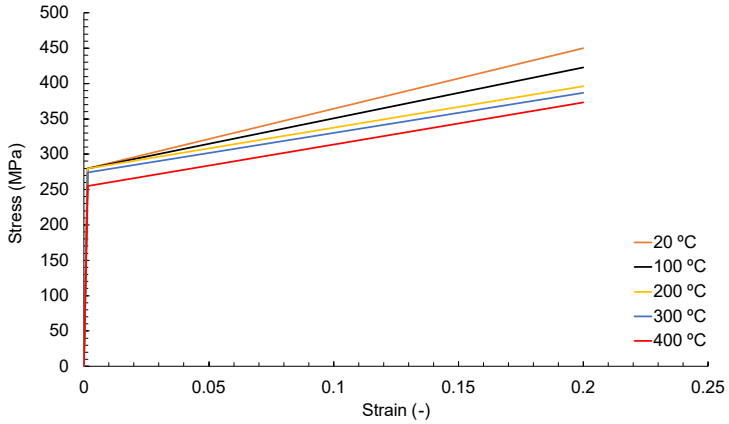

Figure 33 - Stress-strain relationship of steel at various temperatures (Taken from Eurocode 3 Part 1-2).

From the temperature distribution results presented in earlier sections, the operating temperature of the steel shell is around 300 ºC. However, to be conservative and for simplicity, for this analysis, the temperature was assumed to be 400 ºC. Figure 34 shows the results obtained for the nonlinear buckling analysis for the steel shell under gravity loading. Figure 34a shows that the steel shell's elastic limit is much higher than the calculated value of gravity load experienced by the steel shell (15 kN).

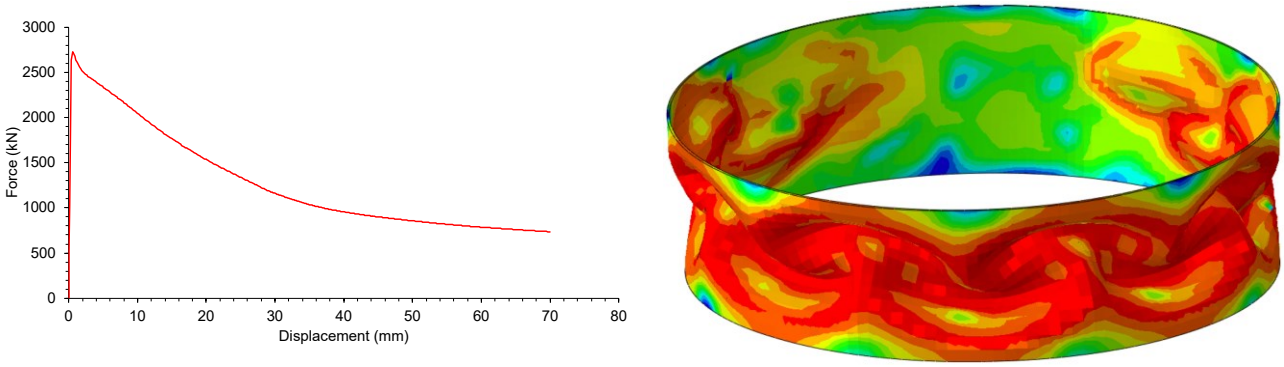

(a) (b)

Figure 34 - Nonlinear buckling analysis for the steel shell under gravity loading:
a) Force-displacement relationship; b) deformed steel shell at 70 mm vertical displacement.

To evaluate the out of plane behaviour of the steel shell due to thermal expansion and mechanical loads imposed by the inner refractory linings, an analysis the of partial ring model with nonlinear properties of steel was carried out. Figure 35 shows the total out of plane displacement observed in the steel shell. The displacement is partially due to thermal expansion and mechanical forces. From Figure 35b, it can be observed that the steel shell does not undergo plasticity for the thermal load application.

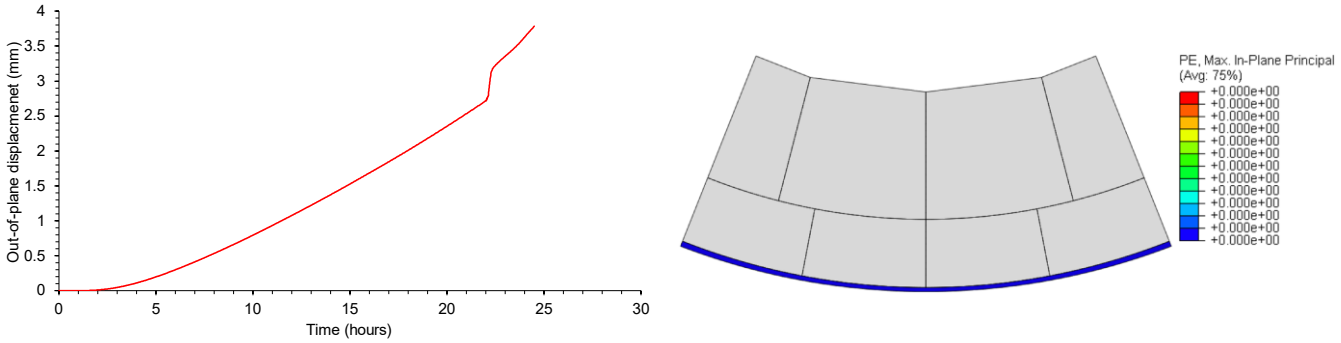

(a) (b)

Figure 35 - Nonlinear analysis of the partial ring model to evaluate out of plane behaviour of steel shell:
a) displacement-time evaluation; b) Plastic strain distribution in a steel shell.

European Commission | Horizon 2020 European Union funding for Research & Innovation

2.7 Final configuration of pilot ladle

From the design optimisation process discussed in the previous sections, the final agreed dimensions of the 3D pilot ladle were 1500 mm diameter and 500 mm height. Figure 36 presents the global overview of the 3D pilot ladle. Different refractory linings are also shown, identical in thickness with an industrial steel ladle. Due to the change in geometry, the bricks in the wear lining will need to be cut. The modified dimensions of the brick and the number of bricks required is also shown in the figure. The shape in the safety and insulating linings do not need to be altered. After converging on the scale of this pilot ladle, the next step is to design the top and bottom insulation by calculating the power required to heat this setup to 1500 ºC and the type and numbers of heating elements necessary to achieve this target. This procedure is discussed in the following section.

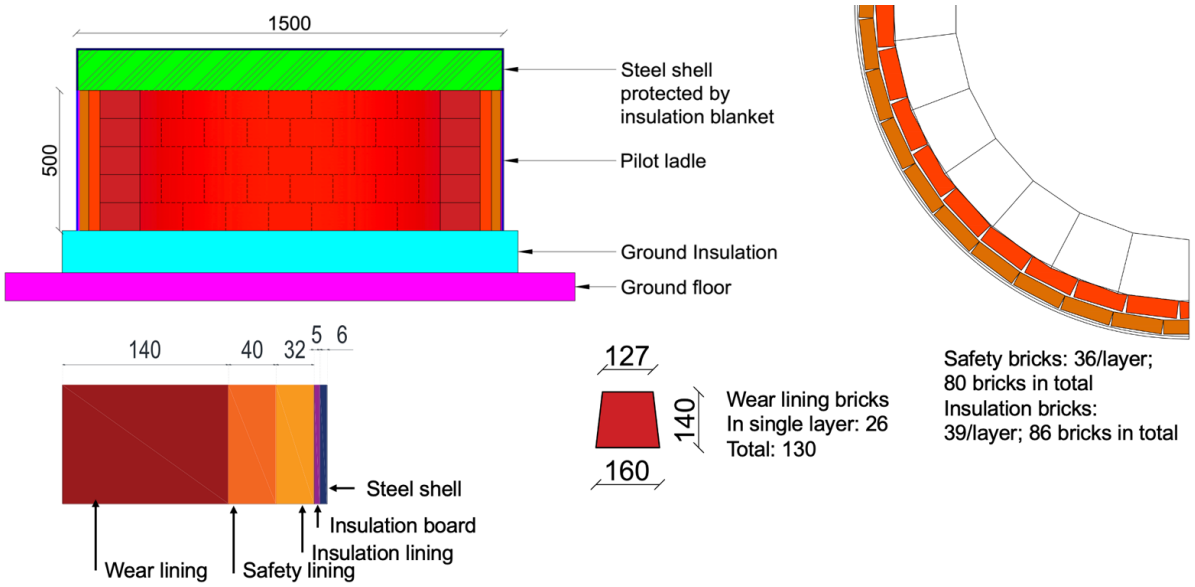

Figure 36 – Graphical illustration of the 3D pilot steel ladle showing the global view, configuration and thickness of the refractory linings and numbers of bricks required for the construction.

3 Design of insulation and heating elements

Insulation layers at the top and bottom of the pilot ladle are essential to reduce heat losses. Additionally, the bottom insulation layer is required to support the weight of the pilot ladle and top insulation layer. Due to size constrains in the laboratory, the pilot ladle should be kept in such a manner that it can be moved if required. Considering these aspects, it was decided to build a steel frame (Figure 37) to support the pilot ladle. With this, it can be moved around, and it can help protect the ground floor of the laboratory from high temperatures. This frame has three main rectangular steel sections on which square steel beams are welded. Above this, triangular steel plates of 6 mm thickness are laid with an allowance for expansion. To support the pilot ladle, insulation bricks (200 mm height) will be laid on these steel plates.

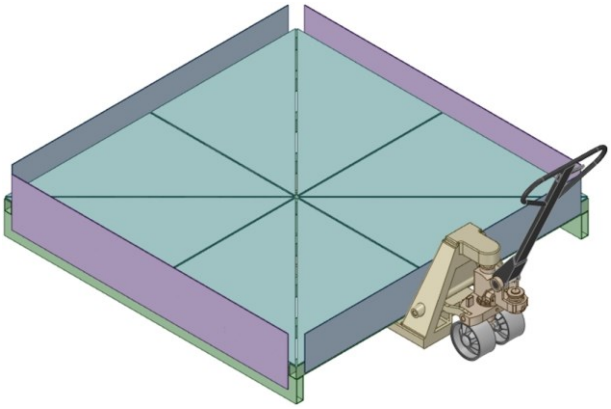

Figure 37 - Steel frame for the bottom insulation layer.

The top insulation layer should be able to withstand the high temperature as well the weight of the heating elements. Additionally, it should be easy to move as well. Different considerations were made for this top insulation layer. For the shape, a flat layer and a dome-shaped layer was considered. Figure 38 shows the distribution of Von Mises stresses in the top insulation layer for two

European Commission | Horizon 2020 European Union funding for Research & Innovation

different shapes. It was observed that the dome-shaped lid imposes a horizontal thrust on the pilot ladle, resulting in more surface area, which will result in higher heat losses. It was agreed to build a flat top lid with a steel shell, and the insulation will be put in place. The chosen thickness of insulation is 200 mm. this was done by considering the heat loss, surface temperature of the steel shell and total weight of the insulation.

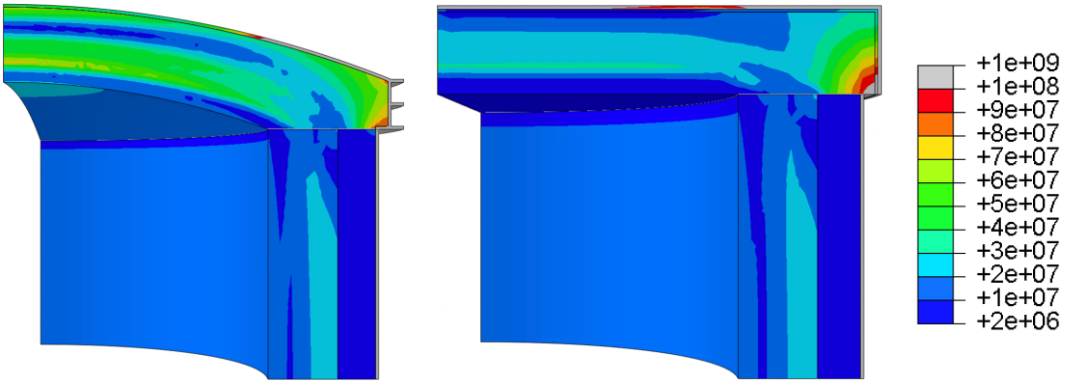

Figure 38 - Design of top insulation layer – distribution of Von Mises stress [Pa]: a) Dome-shaped li; b) Flat lid.

For simplicity in design, the mechanical contribution of insulation was not considered for the top lid. Only the contribution of the steel shell was considered. Figure 39 shows the graphical representation of the top lid. The thickness of the steel shell is 6mm with a diameter of 1612 mm. Three stiffeners were considered to increase the lid's stiffness and reduce the vertical displacement during service conditions. In these top lids, holes will be made to place the heating elements (which are discussed in **Error! Reference source not found.**), and a rectangular window is made to allow monitoring (section **Error! Reference source not found.**).

This top lid will be subjected to two support conditions. It will be supported from the top with a hook during lifting and placing. During service conditions (i.e. during the experiment), it will be supported by the refractory linings of the pilot ladle. Considering these support conditions, a nonlinear analysis was carried out to evaluate its behaviour. Figure 40 shows the behaviour of the steel shell subjected to different support conditions. The diagram indicates that the steel shell's elastic load carrying capacity is much higher than its self-weight, weight of the insulation, and heating elements (10 kN).

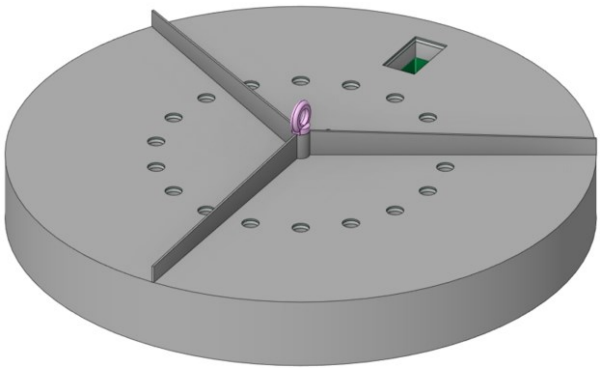

Figure 39 - Top lid of the pilot ladle.

European Commission
Horizon 2020
European Union funding
for Research & Innovation

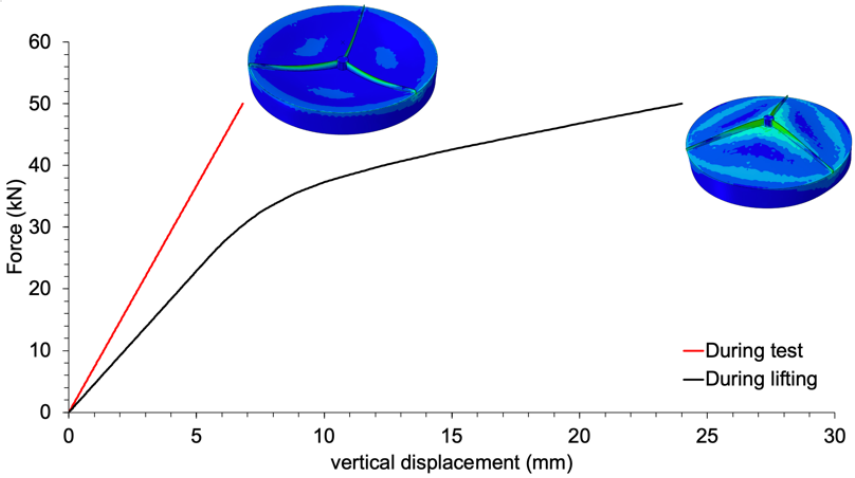

Figure 40 - Force-displacement diagram of the top steel shell subjected to different support conditions during testing and during lifting of the lid.

An assessment of the electrical power requirement is crucial for the experiments on the pilot steel ladle. From this calculation, the number of heating elements required can be calculated. This number should also validate the capacity of the existing power supply unit. For this purpose, transient heat transfer analyses were carried out considering various heating rates (from 1 ºC/min to 3 ºC/min) and with different heat transfer coefficients for the hot face surfaces (from 50 W/m^{2}K to 1000 W/m^{2}K). This was done to capture all possible aspects of thermal loadings. Figure 41 presents an example of such analysis with a 2 ºC/min thermal loading rate and a heat transfer coefficient of 300 W/m^{2}K. Figure 41a shows the temperature distribution in the refractory linings and insulation layers. The temperature distribution in refractory linings of the pilot ladle (Figure 41c) is similar to the observed distribution in partial ring models. Figure 41b illustrates the hot and cold face surfaces considered for the flux calculation. The power requirement during heating and steady state is shown in Figure 41d. This figure indicates a maximum power of 46 kW during heating and 21.5 kW during steady state.

All analyses considering different parameters found that the steady-state power consumption is 21.5 kW for all the cases. The maximum power requirement varies with the heating rate and heat transfer coefficient. It is possible to achieve a surface temperature of 1450 ºC with this insulation setup and power requirement. These results and consultations with the heating element suppliers determined the number of the heating element and its spacing. Eighteen silicon carbide heating elements (Kanthal Globar SR as shown in Figure 42) will be placed 138 mm away from the surface of the wear lining. The spacing between the elements is also 138 mm (Figure 39).

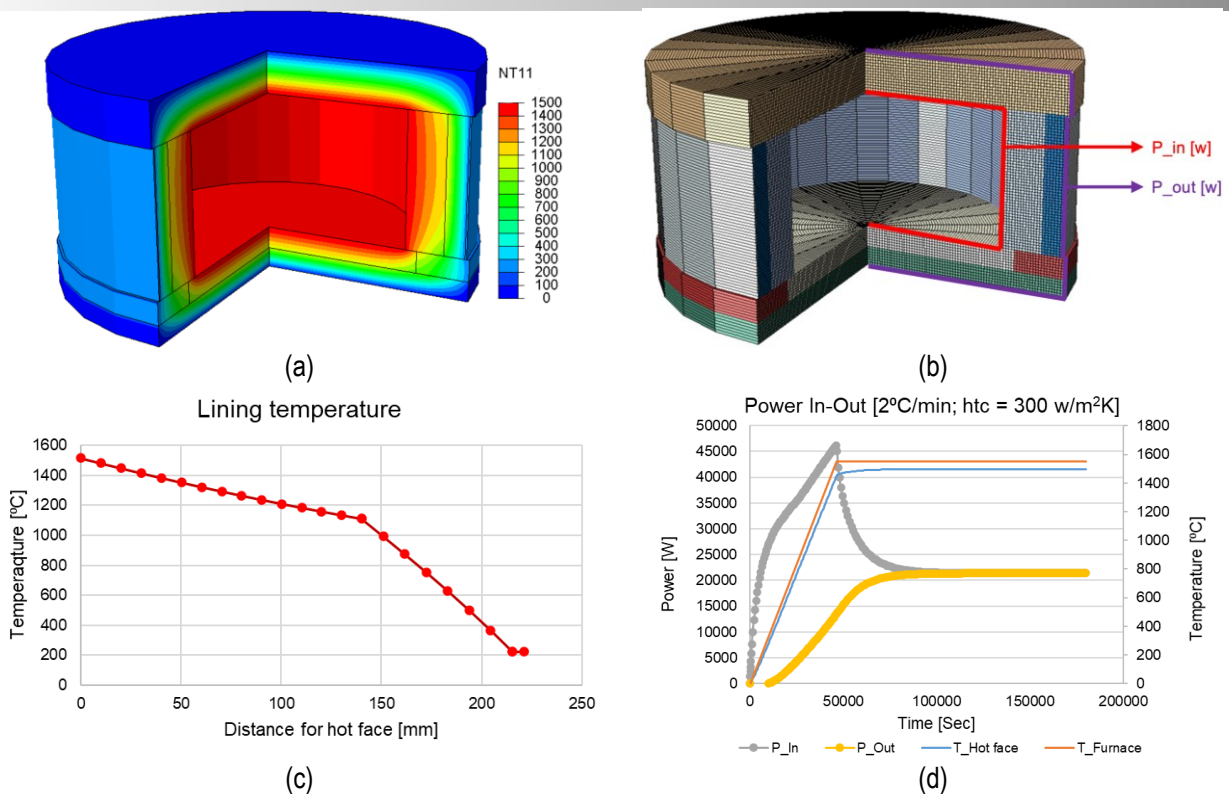

Figure 41 – Power requirement calculation for pilot steel ladle: a) temperature distribution during steady-state; b) Finite element model with lines showing surface area used for the calculation of total heat flux; c) temperature distribution in the lining; d) Chart showing power requirement during heating and steady-state.

Figure 42 - Silicon carbide heating element (Kanthal Globar SR) with a heating length of 450 mm.

4 Experimental outputs

Experiments on the pilot model will be performed to observe the behaviour of refractory linings at elevated temperatures. Thus, it is expected to measure the temperature distribution, strains and dry joint opening and closing. These measurements are important for the calibration and validation of the developed numerical models. The temperature distribution will assist in identifying key thermal boundary parameters, such as heat transfer coefficient, and emissivity at the exposed surfaces of the linings. Additionally, the temperature measurements acquired within the surface will help to reconfirm the thermal properties of the material (i.e., thermal conductivity and specific heat). Another key aspect in the validation of the numerical models is definition of the local mechanical boundary conditions (i.e., interaction between the bricks and linings). Thus, measurement obtained for that definition is of importance. Moreover, the measurement of the mechanical fields (strain and displacement) will assist in confirming the thermomechanical properties of the material (thermal elongation, elastic-viscoplastic behaviour and damage). Therefore, identifying suitable measurement devices is necessary so that reliable data can be used to calibrate the numerical model.

Various devices for the acquisition of the thermal and mechanical field were studied within ATHOR project. Deliverable 1.6: instrumentation tools for measurements on industrial devices, provides review of such techniques. That document is taken as a base for the further review of the potential measurement devices, presented in the following section.

4.1 Review of potential measurement devices

While identifying suitable acquisition devices, measurement tools were categorised into two classifications, namely, thermal characterisation tools and mechanical characterisation tools. The evaluation of the temperature fields results in the acquisition of essential information that is required to evaluate the thermal behaviour of the pilot ladle that will operate at high temperatures.

The layers of the refractory lining are composed of different materials with specific properties and are submitted to varying temperatures in service. Possible tools that were identified for the thermal measurements are thermocouples and infrared cameras.

Thermocouples are widely used for the instrumentation of industrial devices [8][9]. The most common K type is composed of Nickel-Chromium / Nickel-Alumel (nickel + aluminium + silicon alloy). This thermocouple is widely used because it is inexpensive, accurate, reliable and can operate in a wide range of temperatures, up to 1260 °C, with an accuracy of +/- 2.2 °C. The thermocouples can be installed at the refractory layers (working, safety and insulation) and in the steel shell at different locations. They can be installed in holes drilled into the refractory bricks or welded to steel parts. Thus, thermocouples can provide temperature measurement within the material. However, thermocouple provides measurement only at the installed location and it is not representative of the distribution over an area.

While the infrared camera is a valuable tool that can measure the temperature distribution on the external surface of the pilot steel ladle from a relatively distance. The infrared camera presents some advantages compared to the use of thermocouples. This equipment provides complete field measurement of the temperatures, while thermocouples provide point measurements. Therefore, if the problem involves a significant gradient of temperatures for large structures, many thermocouples would be necessary to evaluate the system. In contrast, only one IR camera would be required to provide all the required measurements on each surface. A drawback is a limitation on measuring temperatures inside the linings and between the layers, so in such cases, thermocouples are more suitable.

For mechanical devices (i.e. Strain/displacement measurements), Linear Variable Differential Transformer (LVDT), Strain gauges, Fiber Bragg grating (FBG), Marker tracking, Digital Image correlation, Laser scanning and Photogrammetry tools were identified. The LVDTs, strain gauges and FBGs requires installation on the surface. While other techniques of strain/displacement field measurements are remote and does not require contact with the surface. For measurements in a high-temperature application, choice of contact and contactless techniques is crucial. Devices requiring contact needs to work well at high-temperatures and contactless devices requires a clear field of view of the measurement surfaces.

LVDTs are robust and reliable instrument for measuring linear displacements. LVDTs are widely used in different field of research, particularly in civil and mechanical engineering due to its low hysteresis and excellent repeatability. However, the commercially available LVDTs are designed to operate up to 650 °C. For a high-temperature application, LVDTs requires extension with a ceramic material (usually high alumina tubes). This configuration could be used for hot face of the working lining in the pilot ladle, however, it would require a direct access from the top lid for placement. Moreover, the measurement acquired from this instrument is linear displacement between two points.

Strain gauges are widely used for the point measurement of strain over a surface in many applications. Considering the material of the measurement surface, size of the gauge varies. Strain gauges are installed on a surface either with adhesives or spot welded. Commercially available strain gages are able to operate till 650 °C. However, it requires a welded connection with a surface. In this case, this could be useful for the outer steel shell.

Fibre Bragg gratings (FBG) consist of distributed Bragg reflectors constructed over a defined segment of optical fibre that reflects particular wavelengths of lights and transmits all other. Depending on the installation techniques, FBGs can provide temperature measurement or strain measurement over a point. Especially available FBGs can operate till 900 °C (for temperature or strain measurement) or 1200 °C (for temperature measurement only). However, this requires a special coating over the optical fibre and installation of such FBGs over a non-metallic surface is complex, especially at higher temperature.

Marker tracking is a photo-mechanical technique that tracks markers previously installed on the sample's surface. It may determine displacements and strain fields during a thermomechanical solicitation. It is a powerful technique, as it is simple, fast to use, and it requires small computational resources for the data post-processing [14]. Nevertheless, this technique is not suitable to represent discontinuities, such as joints or cracks during high temperature applications.

Digital Image Correlation is an optical full-field measurement technique. It was created at the beginning of the 1980s and has been continuously developed since then, presenting a significant increase in accuracy. It allows the determination of an entire experimental field of strains and displacements based on the grey level conservation principle [15]-[18]. In this case, and depending on the available free fields of view, this could be useful to use.

Photogrammetry is the process of generating 3D models from a series of images of the object; the resulting model can be scaled and used to measure distances between objects and to measure the deformed configuration of some structure. This technique provides reliable measurements at a low-cost [19][20]. The Terrestrial Laser Scanners (TLS), or 3D Scanning, could be used for high-resolution mapping of industrial vessels and equipment [22]. Laser scanning can also be used to measure temperature. Some systems are also able to measure the reduction of the thickness of the linings, as bricks are continuously subjected to corrosive attacks by hot liquid steel and slag. The laser scanner measurements can evaluate the thickness variation of the bricks

in hot conditions by sending infrared laser pulse from outside the ladle to the wall and the bottom. For our case, these techniques could be used to assess the relative geometry of the working lining before and after testing.

4.2 Acquisition systems for 3D pilot ladle

All the measurement techniques discussed in previous section have its merit and demerit. Therefore, selection of these system for the pilot ladle needs to consider the same. Measurement devices employed for the pilot ladle should be able to obtain essential thermomechanical data required for the validation of the numerical modelling. Simultaneously, the selected devices should be such that they are easily available in a reasonable timeframe and within allocated budget. Additionally, such devices should be less intrusive (to limit heat losses) and have high repeatability. Considering all these aspects, several acquisition systems and its potential installation layout is discussed in following sections.

4.2.1 Thermal measurements

The most reliable devices for the thermal measurements are thermocouples and infrared camera. Thermocouples can be installed at various places and infrared camera can be placed outside of the pilot to measure temperature over an area of steel shell. For this, it was decided to place 18 thermocouples in the refractory linings and steel shell at various locations, covering all different layers, as presented in Figure 43. Additional thermocouples will be placed inside top and bottom insulation layers to monitor the heat losses. Therefore, combinations of these two devices can validate the numerical heat transfer models with experimental data.

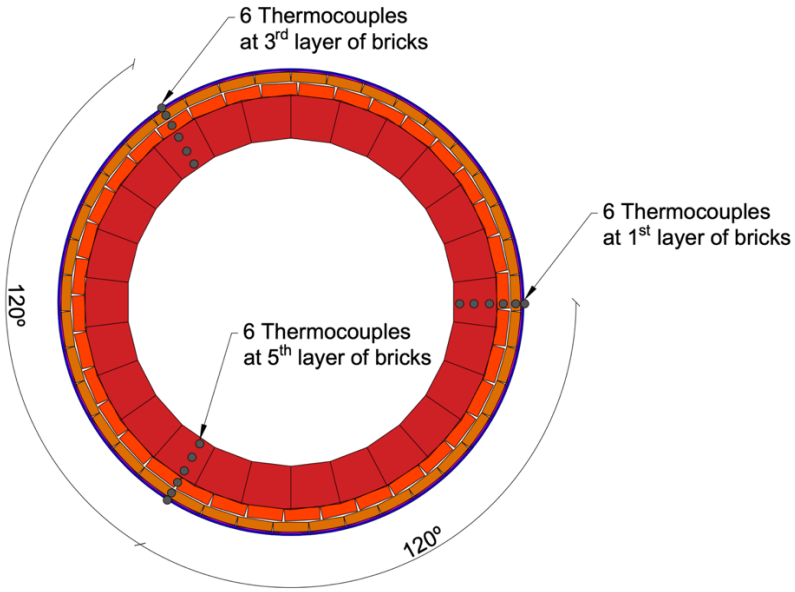

Figure 43 - Placement of thermocouples to measure thermal fields in the various refractory linings and steel shell.

From the installed thermocouples, it will be possible to collect the temperature profile along the different refractory lining at any given time (Figure 44) and during various stages of thermal loading. This data will be used to calculate the thermal loading parameters at the hot and cold face (i.e., heat transfer coefficient and emissivity) and between different refractory linings. This data can be used to calibrate the thermal properties of the various materials with numerical simulations.

European Commission | Horizon 2020 European Union funding for Research & Innovation

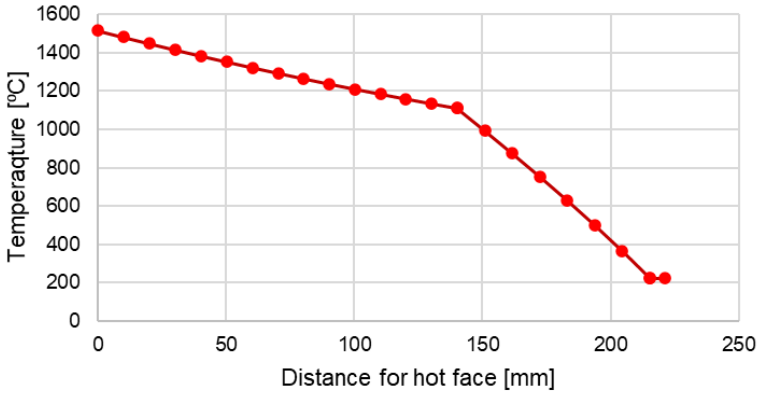

Figure 44 - Example of temperature distribution in the refractory linings for the pilot steel ladle during constant furnace temperature of 1500 ºC.

4.2.2 Mechanical measurements

For mechanical measurement, the most reliable and robust device that requires contact, for high-temperature applications is spot welded strain gauges on the steel shell. Photogrammetry or laser scanning for the hot face is not practical, primarily due to the high temperature in the furnace. However, these techniques can be employed to acquire a point cloud before (Figure 45) and after the experiment. Such point clouds will assist in the formulation of the numerical model by providing true global and local geometrical data. The difference between a before and after scan can be useful in observing deformation in the ladle which can validate numerical models.

Figure 45 - Example of photogrammetry on the inner surface of the pilot ladle in its current state.

Marker tracking and DIC are proven for high temperature applications. Therefore, a combination of marker tracking and DIC will be employed to monitor displacement and strains in the second layer of the wear lining through a cut window in the top lid and on the exterior section of a steel shell (Figure 46).

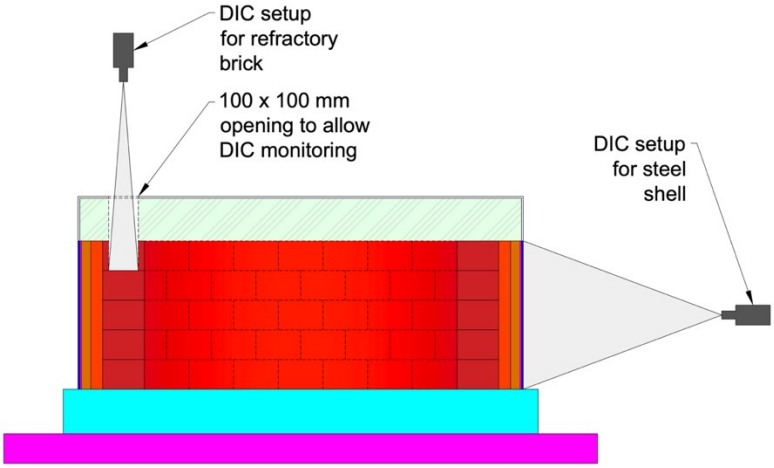

Figure 46 - Placement of DIC setup to measure displacement fields in the top refractory lining layer and steel shell.

To support the results from these remote sensing techniques, ten strain gauges with high-temperature resistance will be used on the cold face of the structure during the experiments where the temperatures will be in the range of 250 ºC (Figure 47). For this

purpose, high-temperature welding foil strain gauges from KYOWA along with a data acquisition system and processing software was acquired. Moreover, extensive before and after manual field measurements, such as Photogrammetry or TLS, will be performed to observe changes in shape, joint thickness, and damage.

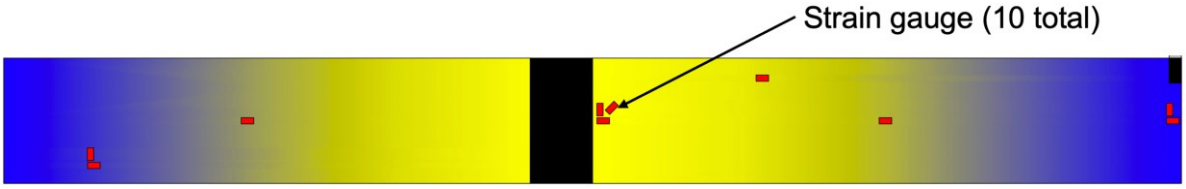

Figure 47 - Placement of weldable strain gauges on the outer surface of the steel shell (the black area in the centre represents the DIC area, and the location on the right represents the DIC setup for refractory).

From the DIC system installed for the refractory linings, it will be possible to collect the strain distribution (Figure 48a) and displacement of the linings (Figure 48b) throughout the experiment. This data will be useful to observe the joint closure behaviour, plasticity, and creep behaviour of the refractories at high temperatures. This data will also be helpful to validate the numerical models of various scales.

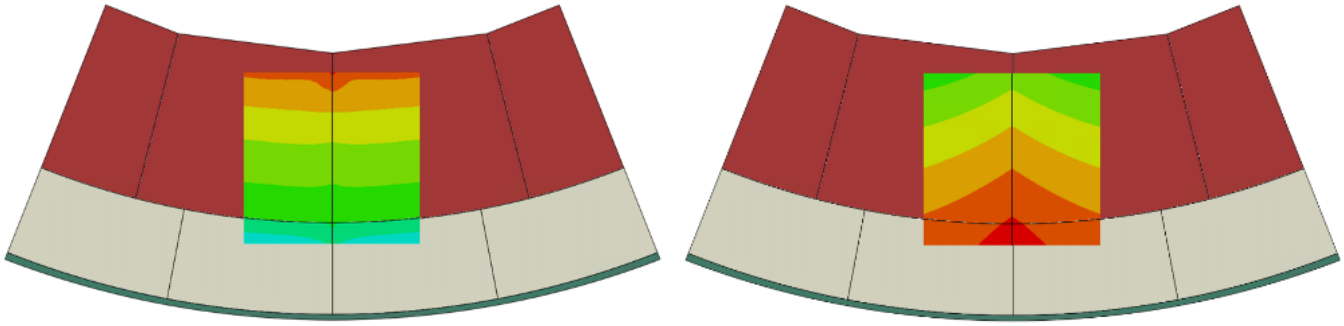

Figure 48 - Example of the DIC measurement for the top lid for refractory linings: a) In-plane strain distribution; b) In-plane displacement distribution.

The strain gauges installed on the outer side of the steel shell along with the DIC setup will be able to provide the development of the strain in the steel shell during the thermal loading as shown in Figure 49. This data along with the parametric numerical simulations will assist in the calculation of the gap between various refractory linings in the pilot steel ladle as the expansion of the steel shell depends on the thermal expansion of the steel shell itself and also the pressure exerted by the inner refractory linings.

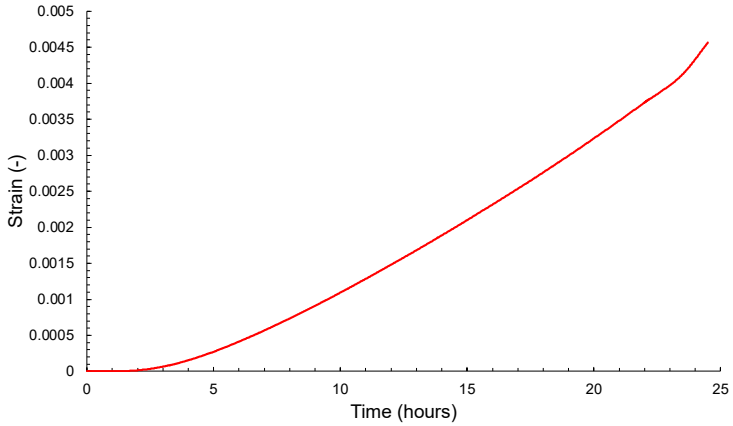

Figure 49 - Example for the development of in-plane total strain in the steel shell of the pilot steel ladle.

5 Current state of the 3D pilot steel ladle

In this section, the current state of the pilot and future actions are discussed. The final configuration of the pilot steel ladle is illustrated in Figure 50. The pilot ladle will be rested on the ground and insulated by two insulation bricks layers. The heating

European Commission | Horizon 2020 European Union funding for Research & Innovation

elements will be placed vertically and are supported by the top lid, which can be easily lifted. These experiments will be carried out at the Ceramics Research Centre of TATA Steel at IJmuiden, Netherlands.

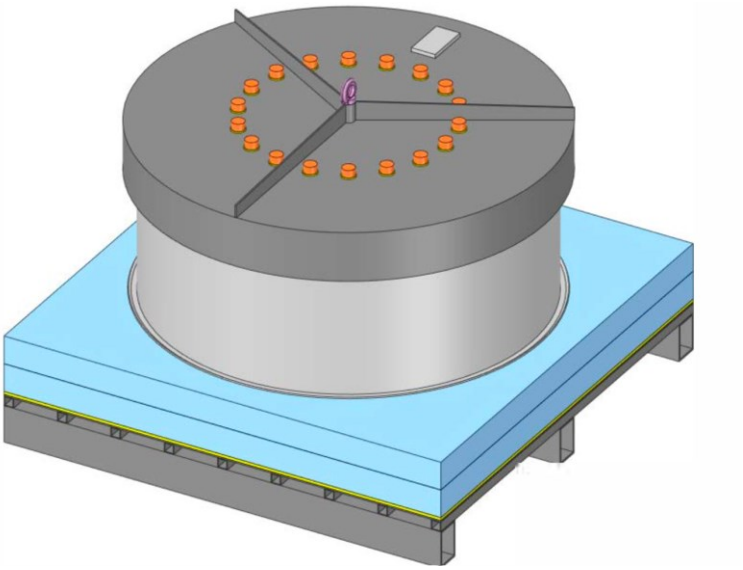

Figure 50 - Graphical representation of the whole assembly for the experiments on pilot steel ladle.

All the steelwork is fabricated and delivered. The first process was to assemble the bottom steel frame components and create a base for the pilot ladle to rest. This process is shown in Figure 51. After the frame was built, it was lined with insulation boards (5 mm thickness) and two lightweight, high insulation bricks with a total thickness of 200 mm.

(a) (b)

Figure 51 - Steel frame for the ground support: a) steel frame components; b) assembly of the steel frame.

Afterwards, the steel shell of the pilot ladle was placed at the centre of the base insulation Figure 52. In this figure, the combined assembly of pilot ladle shell and base insulation can be observed. Currently, the pilot ladle is lined with insulation boards and insulation bricks. This was done to perform an initial check (a trial run) to assess the ability of heating elements to provide a sufficient temperature gradient. The trial run will be performed first with this assembly once all the components are ready.

European Commission | Horizon 2020 European Union funding for Research & Innovation

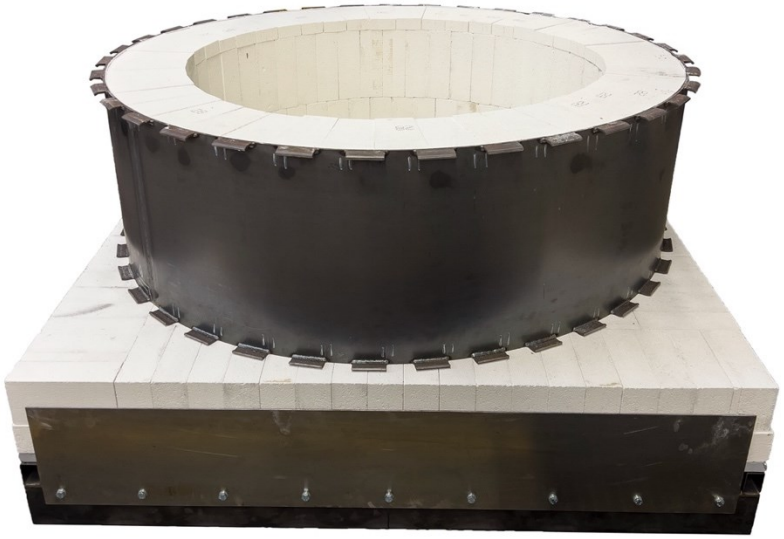

Figure 52 - Pilot steel ladle rested with insulation bricks on the ground support frame. The pilot ladle is lined with insulation boards (5 mm thickness) and insulation bricks.

Another critical aspect was the insulation of the top lid. This task was performed at the steel plant of TataSteel. The casting process is presented in Figure 53. The process involved drilling 18 holes for the placement of the heating elements and cutting a window of 100 × 200 mm^2 for the DIC measurements. Afterwards, the steel anchors were welded to the steel shell to ensure that the insulation material do not fall off during experiments. Once finished, an insulation layer of 5 mm thickness was laid, and the surface was prepared for the casting. The casting was done with a medium weight insulating concrete with a maximum temperature capacity of 1550 ºC. After casting, the top lid was placed in a furnace for 48 hours at 300 ºC for drying and dewatering to remove free and chemically bonded water.

(a) (b) (c)

Figure 53 - Top lid of the pilot steel ladle: a) steel shell with welded anchors, drilled holes for the heating elements and window for DIC measurement being lined with insulation board; b) top lid before casting of insulation concrete; c) top lid after casting.

Currently, all the required components for the experiments are delivered and built. The electrical connection requires an upgrade to ensure a good and constant supply. This task needs to be managed on site (being currently addressed by TataSteel) and the experimental campaigns are scheduled to start as soon after this task is complete.

6 Conclusion

Within ATHOR, an unprecedented experimental installation was developed – a 3D pilot ladle. This represents a novel approach towards designing an experimental setup for large-scale refractory masonry. This campaign makes it possible to investigate

European Commission | Horizon 2020 European Union funding for Research & Innovation

performance in a configuration representing large-scale industrial installations. It will be possible to characterise the behaviour of refractory linings and steel shell from the experimental data while isolating the effect of ladle bottom and molten steel. This characterisation will ultimately provide insights into the thermomechanical behaviour of refractories in a cylindrical shape, such as joint behaviour, the interaction between the linings, creep, plasticity, and damage of the materials.

The present document describes the development of such experimental installation, including all stages of design. It should be noted that the objective was to present within this document all the experimental results obtained with such experimental campaign. However, due to the COVID pandemic, the work within this task was delayed to a point where the experimental results are not available within the timeframe of ATHOR (March 2022). It should be also noted that extra funding was procured to fund the ESR responsible for the development of this work (at UMinho, for 18 extra months). The Partner Organization involved in the development of such application (TataSteel) has also shown great interest in continuing pursuing its successful development. Although the experimental results are not yet available, they will become available after the timeframe of ATHOR.

These results will then be used to calibrate advanced nonlinear micro and macro numerical models. This calibration process will give essential data regarding the influence of different material and geometric parameters on the global behaviour of the pilot ladle. Identifying these critical parameters will validate the numerical models with the industrial steel ladle and assist in optimising the material utilisation of different refractory linings.

7 References

[1] Schacht, C. A., *Refractory lining: Thermomechanical design and applications. Mechanical Engineering*. 1995.

[2] Jin, S., H. Harmuth, and D. Gruber, “Compressive creep testing of refractories at elevated loads—Device, material law and evaluation techniques,” *Journal of the European Ceramic Society*, vol. 34, no. 15, pp. 4037–4042, Dec. 2014, doi: 10.1016/J.JEURCERAMSOC.2014.05.034.

[3] Breder Teixeira, L. *et al.*, “Experimental Investigation of the Tension and Compression Creep Behavior of Alumina-Spinel Refractories at High Temperatures,” *Ceramics*, vol. 3, 2020, doi: 10.3390/ceramics3030033.

[4] Schacht, C. A., *Refractories handbook*, 1st ed. CRC Press, 2004. doi: 10.1201/9780203026328.

[5] Revie, R. W., *Uhlig’s Corrosion Handbook*. 2011. doi: 10.1002/9780470872864.

[6] Andreev, K., S. Sinnema, A. Rekik, S. Allaoui, E. Blond, and A. Gasser, “Compressive behaviour of dry joints in refractory ceramic masonry,” *Construction and Building Materials*, vol. 34, pp. 402–408, Sep. 2012, doi: 10.1016/J.CONBUILDMAT.2012.02.024.

[7] Oliveira, R. L. G., J. P. C. Rodrigues, J. M. Pereira, P. B. Lourenço, and H. Ulrich Marschall, “Normal and tangential behaviour of dry joints in refractory masonry,” *Engineering Structures*, vol. 243, p. 112600, 2021, doi: 10.1016/j.engstruct.2021.112600.

[8] Oliveira, R. L. G., J. P. C. Rodrigues, J. M. Pereira, P. B. Lourenço, and H. U. Marschall, “Thermomechanical behaviour of refractory dry-stacked masonry walls under uniaxial compression,” *Engineering Structures*, vol. 240, no. December 2020, 2021, doi: 10.1016/j.engstruct.2021.112361.

[9] Prietl, T., “Ermittlung materialspezifischer Kennwerte von feuerfesten Werkstoffen und Zustellungen unter uni- und biaxialen Lastbedingungen für die Nichteisenmetallindustrie,” 2006.

[10] Oliveira, R., J. P. Rodrigues, J. Pereira, P. Lourenco, and R. Lopes, “Experimental and numerical analysis on the structural fire behaviour of three-cell hollowed concrete masonry walls,” *Engineering Structures*, vol. 228, p. 111439, 2021, doi: 10.1016/j.engstruct.2020.111439.

[11] Smith, M., *ABAQUS/Standard User’s Manual, Version 2019*. United States: Dassault Systèmes Simulia Corp, 2019.

[12] Vitiello, D., “Thermo-physical properties of insulating refractory materials,” Ph.D thesis, Université de Limoges, 2021.

[13] Kaczmarek, R., “Mechanical characterization of refractory materials,” Ph.D thesis, Université de Limoges, 2021.

[14] Roselli, I., G. de Canio, M. Rossi, C. Calderini, and S. Lagomarsino, “Relative displacements of 3D optical markers for deformations and crack monitoring of a masonry structure under shaking table tests,” *International Journal of Computational Methods and Experimental Measurements*, vol. 7, no. 4, pp. 350–362, Oct. 2019, doi: 10.2495/CMEM-V7-N4-350-362.

[15] Besnard, G., F. Hild, and S. Roux, “‘Finite-element’ displacement fields analysis from digital images: Application to Portevin-Le Châtelier bands,” *Experimental Mechanics*, 2006, doi: 10.1007/s11340-006-9824-8.

[16] Kaczmarek, R., J. C. Dupré, P. Doumalin, O. Pop, L. Teixeira, and M. Huger, “High-temperature digital image correlation techniques for full-field strain and crack length measurement on ceramics at 1200°C: Optimization of speckle pattern and

uncertainty assessment," *Optics and Lasers in Engineering*, vol. 146, p. 106716, Nov. 2021, doi: 10.1016/J.OPTLASENG.2021.106716.

[17] Teixeira, L., J. Gillibert, T. Sayet, and E. Blond, "A creep model with different properties under tension and compression — Applications to refractory materials," *International Journal of Mechanical Sciences*, vol. 212, p. 106810, Dec. 2021, doi: 10.1016/J.IJMECSCI.2021.106810.

[18] Gabrielli, E. and C. Colla, "Monitoring of masonry compression tests in the lab via optical correlation without surface preparation," in *Key Engineering Materials*, 2015, vol. 624, pp. 139–146.

[19] Mandelli, A., F. Fassi, L. Perfetti, and C. Polari, "Testing different survey techniques to model architectonic narrow spaces," 2017. doi: 10.5194/isprs-archives-XLII-2-W5-505-2017.

[20] Napolitano, R. and B. Glisic, "Methodology for diagnosing crack patterns in masonry structures using photogrammetry and distinct element modeling," *Engineering Structures*, vol. 181, pp. 519–528, Feb. 2019, doi: 10.1016/J.ENGSTRUCT.2018.12.036.

[21] Riveiro, B., P. Morer, P. Arias, and I. de Arteaga, "Terrestrial laser scanning and limit analysis of masonry arch bridges," *Construction and Building Materials*, vol. 25, no. 4, pp. 1726–1735, Apr. 2011, doi: 10.1016/J.CONBUILDMAT.2010.11.094.

[22] Lamm, R. and S. Kirchhoff, "Optimization of ladle refractory lining, gap and crack detection, lining surface temperature and sand-filling of the ladle-taphole by means of a 3D-laserprofile-measurement system that is immersed into a hot ladle to evaluate the entire condition," 2017.